



1

2 **A 1.5-Million-Year Record of Orbital and Millennial Climate** 3 **Variability in the North Atlantic**

4

5 David A. Hodell¹, Simon J. Crowhurst¹, Lucas Lourens², Vasiliki Margari³, John Nicolson¹,
6 James E. Rolfe¹, Luke C. Skinner¹, Nicola Thomas¹, Polychronis C. Tzedakis³, Maryline J.
7 Mleneck-Vautravers¹, Eric W. Wolff¹

8 ¹Godwin Laboratory for Palaeoclimate Research, Department of Earth Sciences, University of Cambridge,
9 Cambridge, CB2 3EQ, UK

10 ²Department of Earth Sciences, Faculty of Geosciences, Utrecht University, Budapestlaan 4, 3584 CD Utrecht,
11 Netherlands

12 ³Environmental Change Research Centre, Department of Geography, University College London, London, WC1E
13 6BT, UK

14 *Correspondence to:* David A. Hodell (dah73@cam.ac.uk)

15 **Abstract.** Climate during the last glacial period was marked by abrupt instability on millennial
16 time scales that included large swings of temperature in and around Greenland (Daansgaard-
17 Oeschger events) and smaller, more gradual changes in Antarctica (AIM events). Less is
18 known about the existence and nature of similar variability during older glacial periods,
19 especially during the early Pleistocene when glacial cycles were dominantly occurring at 41-
20 kyr intervals compared to the much longer and deeper glaciations of the more recent period.
21 Here we report a continuous millennially-resolved record of stable isotopes of planktic and
22 benthic foraminifera at IODP Site U1385 (the “Shackleton Site”) from the southwestern Iberian
23 margin for the last 1.5 million years, which includes the Middle Pleistocene Transition (MPT).
24 Our results demonstrate that millennial climate variability (MCV) was a persistent feature of
25 glacial climate, both before and after the MPT. Prior to 1.2 Ma in the early Pleistocene, the
26 amplitude of MCV was modulated by the 41-kyr obliquity cycle and increased when axial tilt
27 dropped below 23.5° and benthic $\delta^{18}\text{O}$ exceeded $\sim 3.8\text{‰}$ (corrected to *Uvigerina*), indicating a
28 threshold response to orbital forcing. Afterwards, MCV became focused mainly on the
29 transitions into and out of glacial states (i.e., inceptions and terminations) and during times of
30 intermediate ice volume. During the MPT (1.2–0.65 Ma), obliquity continues to modulate the
31 amplitude of MCV but in a more non-linear fashion as evidenced by the appearance of
32 multiples (82, 123 kyrs) and combination tones (28 kyrs) of the 41-kyr cycle. At the end of the
33 MPT (~ 0.65 Ma), obliquity modulation of MCV amplitude wanes as quasi-periodic 100-kyr
34 and precession power increase, coinciding with growth of oversized ice sheets on North
35 America and the appearance of Heinrich layers in North Atlantic sediments. Whereas the



36 planktic $\delta^{18}\text{O}$ of Site U1385 shows a strong resemblance to Greenland temperature and
37 atmospheric methane (i.e., northern hemisphere climate), millennial changes in benthic $\delta^{18}\text{O}$
38 closely follow the temperature history of Antarctica for the past 800 ka. The phasing of planktic
39 and benthic $\delta^{18}\text{O}$ throughout much of the record is similar to that observed for MIS 3, which
40 has been suggested to mimic the signature of the bipolar seesaw -- i.e., an interhemispheric
41 asymmetry between the timing of cooling in Antarctica and warming in Greenland. The Iberian
42 margin isotopic record suggests bipolar asymmetry was a robust feature of interhemispheric
43 glacial climate variations for at least the past 1.5 Ma despite changing glacial boundary
44 conditions. A strong correlation exists between millennial increases in planktic $\delta^{18}\text{O}$ (cooling)
45 and decreases in benthic $\delta^{13}\text{C}$, indicating millennial variations in North Atlantic surface
46 temperature are mirrored by changes in deep-water circulation and remineralization of carbon
47 in the abyssal ocean. We find strong evidence that climate variability on millennial and orbital
48 scales are coupled across different time scales and interact, in both directions, which may be
49 important for linking internal climate dynamics and external astronomical forcing.

50

51 **1. Introduction**

52

53 **1.1 History of Millennial Climate Variability**

54

55 Millennial climate variability (MCV) is operationally defined as having a recurrence time
56 between 10^3 and 10^4 years. It excludes variation on orbital timescales but may include
57 harmonics or combination tones of the orbital cycles that have a period of $<10,000$ years
58 (Berger et al., 2006). MCV is part of the background spectrum of climate variability that
59 follows a power law connecting annual to orbital timescales (Huybers and Curry, 2006). MCV
60 shows closer relationships to Milankovitch cycles than to higher frequency cycles or
61 oscillations (Huybers and Curry, 2006) and some MCV may result from non-linear coupling
62 of processes operating on orbital time scales (Hagelberg et al., 1994). Because climatic
63 processes are intimately linked across different time scales, documenting the long-term history
64 of MCV is important for understanding its relationship to orbitally-forced changes in
65 Quaternary climate.

66

67 The first millennial event to be widely recognized in paleoclimate records was the Younger-
68 Dryas when a 1,300-yr-long period of cold climate began at 12,800 yrs BP and reversed the
69 general warming trend of the last deglaciation in the Northern Hemisphere (for a review, see
70 Mangerud, 2021). Further study of Greenland ice cores revealed the common occurrence of
71 similar abrupt warming/cooling events during Marine Isotope Stage (MIS) 3 (~57 to 29 ka).



72 These Dansgaard-Oeschger (D-O) events represent the rapid switching of North Atlantic
73 climate between colder stadial and warmer interstadial states in less than 100 years with a
74 recurrence time of ~1500 years (Dansgaard et al., 1982). The discovery of such abrupt climate
75 changes in Greenland in the early 1980s was unexpected because of the great magnitude and
76 rapidity of the temperature change and short recurrence times.

77
78 Following the recognition of MCV in Greenland, the search began to see if similar events were
79 recorded in marine sediment cores in the North Atlantic. Marine evidence for D-O events was
80 found in variations in sediment color and the abundance of the polar foraminifer
81 *Neogloboquadrina pachyderma* (sinistral) at DSDP Site 609 (Broecker et al., 1990; Bond et
82 al., 1992, 1993). During some of the most extreme stadial events, North Atlantic marine
83 sediment cores were also found to contain layers of ice-rafted detritus (IRD) that are rich in
84 detrital carbonate derived from Paleozoic bedrock underlying Hudson Strait (Heinrich, 1988;
85 Broecker et al., 1992; Hemming, 2004). These so-called 'Heinrich events' were attributed to
86 massive discharges of the Laurentide Ice Sheet to the North Atlantic via Hudson Strait. The D-
87 O cycles are packaged into longer-term cycles ("Bond cycles") where the amplitude and
88 duration of stadial-interstadial events decrease as climate become progressively cooler until
89 terminating in a Heinrich stadial, which is followed by a large abrupt warming (Bond et al.,
90 1993). The recurrence time of Bond cycles and Heinrich events is on the order of every ~7-8
91 kyrs, which is longer than D-O events.

92
93 MCV, as expressed in Greenland temperature, has a counterpart variation in Antarctic ice cores
94 that is smaller in magnitude and more gradual in nature than the signals found in Greenland.
95 The one-to-one coupling between these events is often explained by changes in inter-
96 hemispheric heat transport referred to as the thermal bipolar seesaw (Bender et al., 1994;
97 Stocker, 1998; Blunier and Brook, 2001; EPICA Community Members, 2006; WAIS Divide
98 Project Members, 2015). The duration of stadials in Greenland is linearly correlated with the
99 strength of warmings in Antarctica (EPICA Community Members, 2006; WAIS Divide Project
100 Members, 2015). The longer-duration interstadials in Antarctica (Antarctic Isotope Minimum
101 or AIM events) are also marked by rises in atmospheric CO₂ (Ahn and Brook, 2014; Bauska et
102 al., 2021), presumably from decreased stratification and increased overturning in the Southern
103 Ocean (Anderson et al. 2009; Skinner et al., 2010, 2020). On millennial time scales, CO₂
104 closely tracks Antarctic temperature with peak CO₂ levels lagging peak Antarctic temperature
105 by more than 500 years (Bauska et al., 2021). The magnitude of the CO₂ rise is correlated with



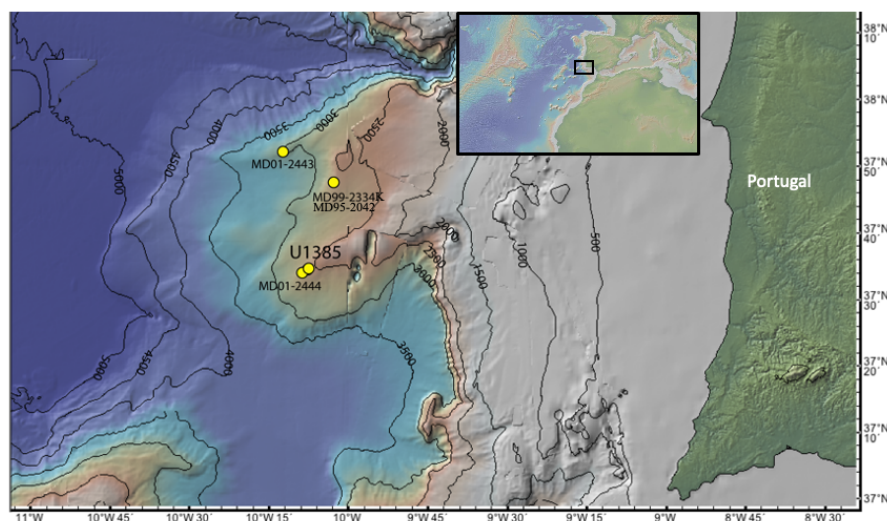
106 the duration of the North Atlantic stadial stage (Buizert and Schmittner, 2015), with a greater
107 CO₂ response during times of prolonged stadial conditions in Greenland, such as those
108 associated with Heinrich events. These longer-lived millennial events represent major
109 reorganizations of the ocean-atmosphere system and have far-reaching effects well beyond the
110 North Atlantic region.

111
112 A leading hypothesis is that changes in deep-water/ocean circulation have played a key role in
113 MCV (for review, see McManus et al., 2004; Alley et al., 2007; Henry et al., 2016; Lynch-
114 Stieglitz, 2017; Menviel et al., 2020). The Atlantic Meridional Overturning Circulation
115 (AMOC) is sensitive to mode jumps that can be triggered by changes to the surface-water
116 density in North Atlantic source areas of deep-water formation. Climate models of varying
117 complexity have simulated millennial oscillations when forced by freshwater fluxes from
118 melting ice (Stocker and Johnsen, 2003; Ganopolski and Rahmstorf, 2001; Timmermann et al.,
119 2003; Rahmstorf et al., 2005), whereas others have emphasized the role of sea ice (Gildor and
120 Tziperman, 2001; Sevellec and Fedorov, 2015; Li et al., 2005, 2010) and/or ice shelf dynamics
121 (Dokken et al., 2013; Petersen et al., 2013). Some model simulations have shown spontaneous
122 oscillation of the AMOC even in the absence of deliberate fresh-water forcing (Winton and
123 Sarachik, 1993; Sakai and Peltier, 1999; de Verdière, 2007; Kleppin et al., 2015). Others have
124 implicated orbitally-induced insolation changes or variations in atmospheric CO₂ as (external
125 to the North Atlantic) triggers of MCV (Friedrich et al., 2010; Zhang et al., 2021; Yin et al.,
126 2021; Zhang et al., 2017; Vettoretti et al., 2022).

127
128 Oxygen isotope records of foraminifera capable of resolving orbital-scale variations are
129 numerous (for a summary of records and resolutions, see fig. 2 of Ahn et al., 2017), but few
130 long millennial-resolved records exist to examine the interaction between orbital and millennial
131 components of the climate system. The study of long-term changes in MCV requires long
132 continuous sedimentary sequences with high sedimentation rates from climatically sensitive
133 areas of the world ocean. Some marine records of MCV exist beyond the last glacial cycle
134 (McManus et al., 1999; Hodell et al., 2008; Oppo et al., 1998; Kawamura et al., 2017; Jouzel
135 et al., 2007; Loulergue et al., 2008; Barker et al., 2011, 2015; Martrat et al., 2007; Margari et
136 al., 2010; Alonso-Garcia et al., 2011; Burns et al., 2019; Gottschalk et al., 2020), but only a
137 few extend beyond 800 ka into the early Pleistocene (Raymo et al., 1998; McIntyre et al., 2001;
138 Birner et al., 2016; Billups and Scheinwald, 2014; Hodell et al., 2008; Hodell et al., 2015;
139 Hodell and Channell, 2016; Barker et al., 2021, 2022).



140
 141 Here we present a 1.5-million-year record of millennial variability in surface- and deep-water
 142 properties as recorded by stable isotopes of planktic and benthic foraminifera at IODP Site
 143 U1385 (the “Shackleton Site”) located off Portugal in the NE Atlantic Ocean (Fig. 1). The
 144 Iberian margin is a well-known location for sediment cores that capture orbital- and millennial-
 145 scale variations in North Atlantic climate (Shackleton et al., 2000; 2004; Martrat et al., 2007;
 146 Hodell et al., 2013, 2015). Because of its location in the eastern Atlantic at ~37°N, the region
 147 is sensitive to migrations in the Polar Front but is positioned far enough south that proxies don’t
 148 saturate under full glacial or interglacial conditions.



149
 150 **Figure 1.** Location of IODP Site U1385 and selected piston (MD95-2042, MD01-2444,
 151 MD01-2443) and kasten (MD99-2334K) cores on the Promontorio dos Principes de Avis,
 152 along the continental slope of the southwestern Iberian margin. The map was made with
 153 GeoMapApp (www.geomapapp.org) using bathymetry of Zitellini et al. (2009).

154
 155 The long, millennial-resolved isotope records from Site U1385 provide an opportunity to
 156 address several questions about the nature of MCV on orbital and millennial timescales. How
 157 common was MCV during older glacial periods of the Pleistocene? Does the nature (intensity,
 158 duration, pacing) of MCV change with orbital configuration or climate background state (ice
 159 volume, sea-level, ice sheet height)? What is the relationship between MCV and longer-term,
 160 orbitally-driven glacial-interglacial cycles – how do they interact? How did MCV change
 161 across the Middle Pleistocene Transition (MPT) when ice sheets grew larger in size and the
 162 amplitude of glacial-interglacial cycles increased? Was the thermal bipolar seesaw mechanism



active during older glacial periods of the Pleistocene? What role did millennial variability play in atmospheric CO₂ variations or vice-versa?

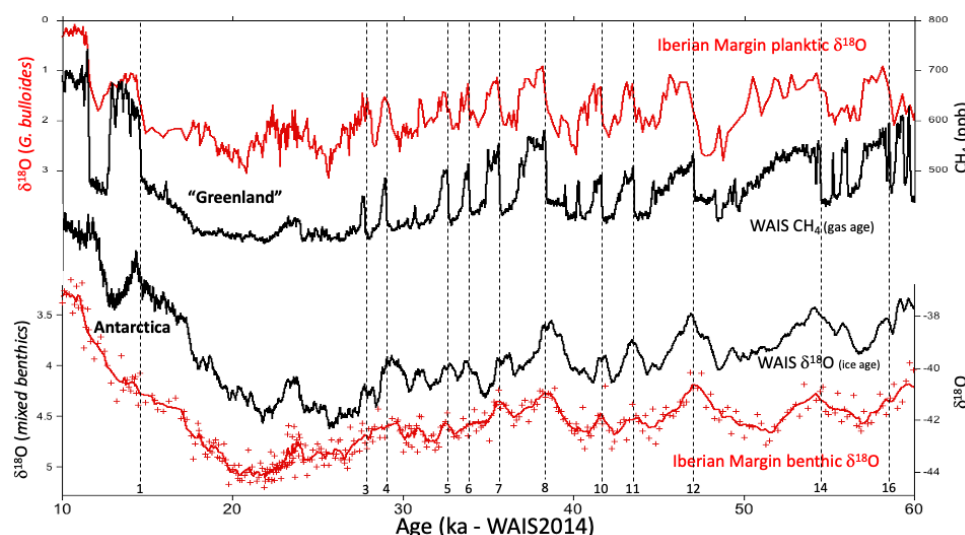
1.2 The Iberian Margin Record

The Greenland and Antarctic ice cores provide continuous paleoclimate records to ~123,000 (NGRIP Project Members, 2004) and 800,000 years (Jouzel et al., 2007) before present, respectively. Beyond the age of the oldest ice, we must rely upon rapidly accumulating marine sediments to document the older history of short-term climate variability in the North Atlantic. Piston cores from the Iberian margin off Portugal contain clear signals of D-O variability in marine sediments (Shackleton et al., 2000, 2004; Martrat et al., 2007; Margari et al., 2010, 2020). High accumulation rates provide the temporal resolution needed to capture the relatively brief, abrupt temperature changes observed in the Greenland ice core. Shackleton et al. (2000, 2004) demonstrated that each of the D-O events in Greenland is expressed in the Iberian margin planktic $\delta^{18}\text{O}$ signal over the last glacial cycle (Fig. 2). In the same sediment core, the benthic $\delta^{18}\text{O}$ signal resembles the δD record in Antarctic ice cores (Shackleton et al., 2000, 2004), capturing each of the Antarctic Isotope Maximum (AIM) events (Jouzel et al., 2007). Because the influence of both Greenland and Antarctic millennial events is co-registered in the same sediment core, the phasing can be determined stratigraphically without the usual limitations associated with determining the absolute ages of short-lived climate events. The observed phasing of isotope signals for the last glacial cycle is consistent with the relative changes in temperature between Antarctic and Greenland deduced from the synchronization of ice core records using methane (Fig. 2) (Blunier and Brook, 2001; WAIS Divide Project Members, 2015). This pattern has been interpreted as a manifestation of the thermal bipolar seesaw (Stocker and Johnsen, 2003) and can be used to recognize a similar mode of operation of the ocean-climate system in older ice cores (Loulergue et al., 2008) and Iberian margin sediment cores (Margari et al., 2010).

The benthic $\delta^{13}\text{C}$ signal of deep cores from the Iberian margin provides a record of changes in the $\delta^{13}\text{C}$ of deep-water dissolved inorganic carbon (DIC), which varies with changes in deep-water source areas, mixing of water masses, and oxidation of organic matter once the water mass is isolated from the surface ocean. In Iberian margin piston cores, surface cooling is associated with systematic decreases in benthic carbon isotopes, indicating concomitant changes in North Atlantic surface temperature and deep-water circulation (Martrat et al., 2007). Cooling is associated with a shoaling of the Atlantic overturning cell that results in a decreased



198 influence of high- $\delta^{13}\text{C}$ North Atlantic Deep Water (NADW) and an increase of southern-
 199 sourced waters with low $\delta^{13}\text{C}$ at abyssal depths in the North Atlantic.
 200



201
 202 **Figure 2.** Comparison of Iberian margin $\delta^{18}\text{O}$ records and polar ice cores. Top panel: Planktic
 203 $\delta^{18}\text{O}$ from core MD95-2042 (Shackleton et al., 2000) compared with CH_4 from the WAIS
 204 Divide ice core on Antarctica (WAIS Divide Project Members, 2015); Bottom panel: benthic
 205 $\delta^{18}\text{O}$ in core MD95-2042 compared with the $\delta^{18}\text{O}$ record of the WAIS Divide ice core (WAIS
 206 Divide Project Members, 2015). Vertical dashed lines are drawn at the abrupt transitions from
 207 cold stadials to warmer interstadial conditions in Greenland and are numbered at the bottom of
 208 the figure. Note that the phasing of planktic and benthic $\delta^{18}\text{O}$ is the same as that inferred from
 209 the CH_4 and $\delta^{18}\text{O}$ in the WAIS Divide ice core. This pattern has been interpreted as being
 210 indicative of a thermal bipolar seesaw.

211
 212 Because of the relative sensitivity of surface and deep-water signals on the Iberian margin to
 213 millennial climate change, this area was targeted by the International Ocean Discovery
 214 Program (IODP) to extend the record beyond the oldest piston cores from the region. In 2011,
 215 five holes were drilled at IODP Site U1385 (the “Shackleton site”) off Portugal, resulting in
 216 the recovery of a continuous 166.5-m sequence. A composite section was constructed by
 217 correlating elemental data measured by core scanning XRF at 1-cm resolution in all holes
 218 (Hodell et al., 2015). The U1385 record extends to 1.45 Ma (MIS 47) with an average
 219 sedimentation rate of 11 cm kyr^{-1} (Hodell et al., 2013; 2015). The record is mostly complete



except for a short hiatus at Termination V that has removed part of late MIS 12 and early MIS 11 (Oliviera et al., 2016).

2. Materials and Methods

2.1 IODP Site U1385 ("Shackleton site")

Site U1385 is located very near the position of piston core MD01-2444 (37° 33.88' N, 10° 8.34' W, 2656 m below sea level; Fig. 1), which consists of a 27-m long sequence representing the last 194 kyr of sediment deposition. Core MD01-2444 can be precisely correlated to Site U1385 on the basis of Ca/Ti measured every 1-cm in both cores (Hodell et al., 2015), thereby providing an equivalent depth (crnmd) in Site U1385 corresponding to each depth in core MD01-2444. Placing MD01-2444 on the Site U1385 depth scale corrects for the well-known effects of stretching and compression that may affect cores recovered with the jumbo Calypso coring system (Skinner and McCave, 2003). Because we did not measure stable isotopes for the upper 23 m of Site U1385 at high resolution, the isotope records presented here consist of a splice between core MD01-2444 (Vautravers & Shackleton 2006; Margari et al., 2010; Hodell et al., 2013; Tzedakis et al., 2018) and Site U1385 (this study). The U1385 record is appended to MD01-2444 at 27.45 m in the piston core which is equivalent to 26 crnmd in Site U1385, corresponding to an age of ~194 kyrs.

Oxygen and carbon isotope measurements of planktic and benthic foraminifera from Site U1385 were made at an average temporal resolution of ~200 years for the last 1.45 million years (Fig. 3). The analytical methods were similar to those described by Hodell et al. (2015). For planktic foraminifera, we used the surface-dwelling species *Globigerina bulloides* from the 250 - 350 μ m size fraction. We interpret the millennial variations in planktic $\delta^{18}\text{O}$ of *G. bulloides* as reflecting variations in sea surface temperature (SST) in the NE Atlantic, which is supported by the strong inverse correlation of planktic $\delta^{18}\text{O}$ and alkenone SST data from Iberian margin cores for the past 400 ka (Martrat et al., 2007). For benthic foraminifera, we used mostly *Cibicidoides wuellerstorfi* and occasionally other species of *Cibicidoides* from the >212 μ m size fraction. In samples where specimens of *Cibicidoides* spp. were absent, we used $\delta^{18}\text{O}$ of *Uvigerina peregrina* or *Globobulimina affinis*. All $\delta^{18}\text{O}$ values for each species were corrected to *Uvigerina* using the offsets suggested by Shackleton et al. (2000) -- i.e., +0.64 for *Cibicidoides* and -0.3 for *G. affinis*. We recognise these offset may vary slightly with time (Hoogakker et al, 2010) but are not large enough to affect the pattern of benthic $\delta^{18}\text{O}$ variation.

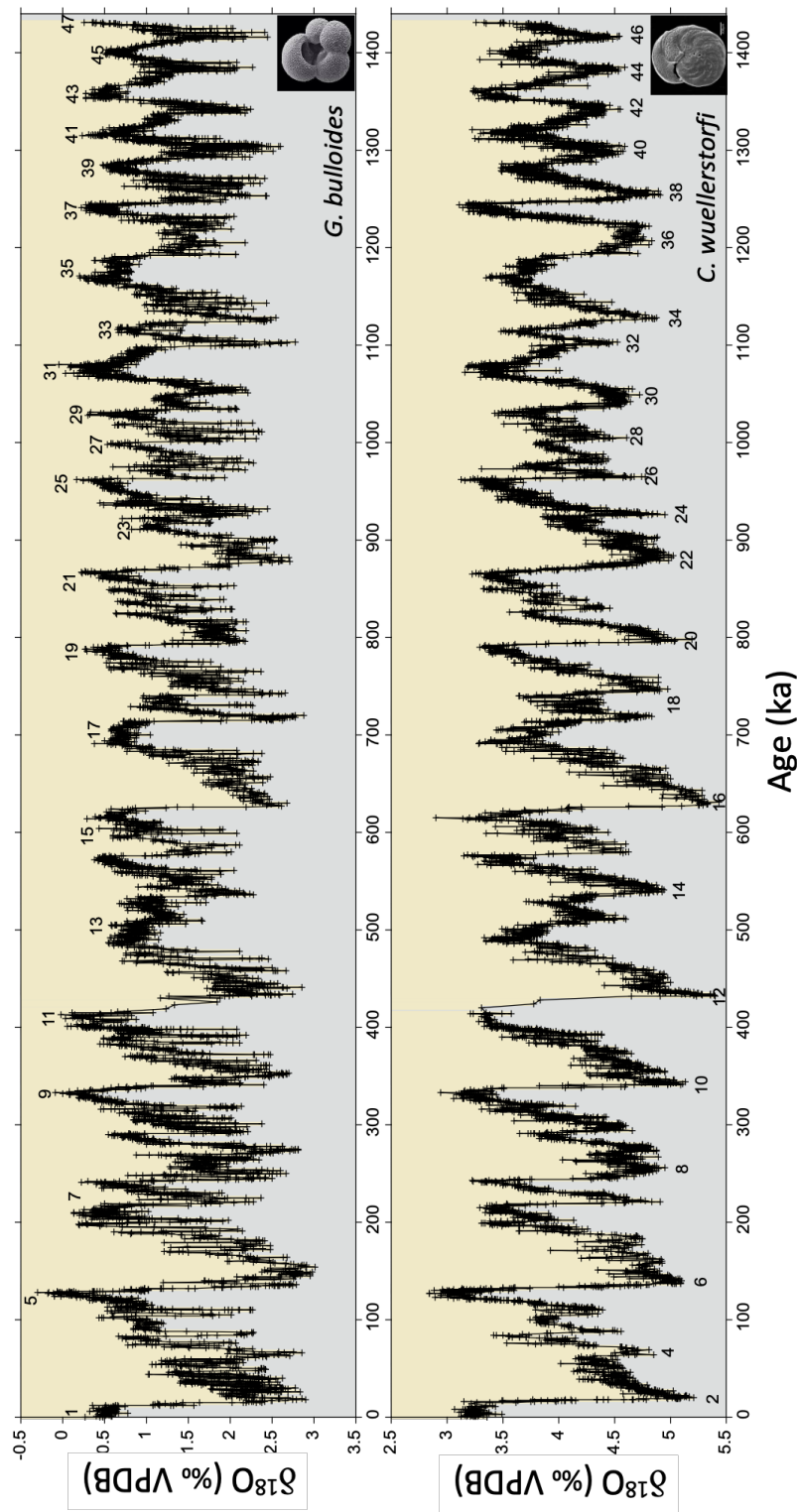


Figure 3. $\delta^{18}\text{O}$ (per mil, VPDB) of the planktic foraminifer *Globigerina bulloides* (top) and benthic foraminifer *Cibicides wuellerstorfi* (bottom) at IODP Site U1385. Interglacial Marine Isotope Stages (MIS) are labeled with odd numbers in top panel and glacial stages with even numbers in bottom panel. Photo credit: *G. bulloides* (<https://www.mikrotax.org/pforams/index.php?id=104034>), *C. wuellerstorfi* (<http://foraminifera.eu/single.php?no=1000394&aktion=suche>)



257 The water depth of Site U1385 (2578 meters below sea level) places it under the influence of
 258 Northeast Atlantic Deep Water today but it was influenced by southern sourced waters during
 259 glacial periods. Variations in benthic $\delta^{18}\text{O}$ reflect changes in temperature and the $\delta^{18}\text{O}$ of
 260 deep water bathing the site, which was affected by ice volume on orbital time scales, albeit
 261 with such ice-volume signals being transported to the core sites on the timescale of ocean
 262 mixing (Duplessy et al., 1991; Skinner et al., 2005; Waelbroeck et al., 2011). Millennial
 263 variations in benthic $\delta^{18}\text{O}$ are affected by changes in deep-water temperature and by the
 264 watermass endmember isotopic compositions (Shackleton et al., 2000; Skinner and
 265 Elderfield, 2003; Skinner et al., 2003, 2007). For benthic $\delta^{13}\text{C}$, we use only the data from the
 266 epibenthic *C. wuellerstorfi* to monitor changes in deep-water ventilation related to changes in
 267 deep ocean circulation and remineralization of organic carbon.

268
 269 Core scanning XRF measurements were made every 1 cm in piston core MD01-2444 (Hodell
 270 et al., 2013) and all holes drilled at Site U1385 (Hodell et al., 2015). The Ca/Ti signal was used
 271 to correlate among holes and define a composite spliced section consisting of intervals from
 272 Holes A, B, D and E to form a total length of 166.5 m. The spliced section used in this study
 273 consists mostly of Holes D and E with a few sections taken from Holes A and B to bridge core
 274 gaps. All sample depths are given in corrected revised meter composite depth (crmcd) that are
 275 corrected for stretching and squeezing caused by coring distortion (Pälike et al., 2005).
 276 Theoretically, the same crmcd should be equivalent in all holes but, in practice, the accuracy
 277 of the alignment among holes is dependent upon the scale of the correlative features and
 278 variability of the Ca/Ti record. We estimate that Ca/Ti features are correlated to the decimeter
 279 level or better.

280
 281 Orbital and millennial variability at Site U1385 is expressed in sediment compositional changes
 282 as reflected by elemental ratios (Hodell et al., 2013, 2015). Detrital sediment supply increases
 283 relative to biogenic production during cold periods, which is reflected in an increase in Zr/Sr
 284 and decrease in Ca/Ti (Hodell et al., 2015), which are inversely correlated with one another.
 285 During the last glacial cycle, increases in Ca/Ti occur during Greenland interstadials whereas
 286 peaks in Zr/Sr mark the stadials, particularly those containing Heinrich events (Channell et al.,
 287 2018).

288
 289
 290
 291
 292



2.2 Chronology

We have updated previous age models of piston core MD01-2444 and IODP Site U1385 (Hodell et al., 2013, 2015) and provide several alternative time scales so users can choose the chronology that is best suited to their specific application. The age models for MD01-2444 include (0 to 194 ka): (1) WAIS Divide (WDC2014) by correlation of planktic $\delta^{18}\text{O}$ to WAIS methane between 10 and 60 kyrs; (2) AICC 2012 for MD01-2444 by correlation of benthic $\delta^{18}\text{O}$ to δD of EPICA from 60 to 135 ka and using the tie points of Shin et al. (2020) from 135 to 190 ka during MIS 6; (3) a Corchia speleothem chronology is provided for MIS 5 by correlation of planktic $\delta^{18}\text{O}$ to the $\delta^{18}\text{O}$ of the stalagmite record (Tzedakis et al., 2018).

The age models from MD01-2444 (0 to 194 ka) are combined with those for Site U1385 (>194 ka) to produce the following chronologies: (1) AICC2012 to 800 ka by iteratively correlating millennial events in Site U1385 planktic $\delta^{18}\text{O}$ to EPICA CH_4 (gas age) and benthic $\delta^{18}\text{O}$ to EPICA δD (ice age), (2) Greenland Synthetic (0-800 ka) by correlation of the planktic $\delta^{18}\text{O}$ to Barker et al. (2011), (3) revised LR04 chronology (Lisiecki and Raymo, 2005) based on correlation of Site U1385 benthic $\delta^{18}\text{O}$ to the Prob Stack (0 to 1450 ka) (Ahn et al., 2007), and (4) an orbitally-tuned time scale by correlation of L^* to the Mediterranean sapropel stratigraphy of the eastern Mediterranean (Konijnendijk et al., 2015). In general, the tuned time scale of Site U1385 compares favorably with LR04 within the estimated error of the chronology, which is ± 4 kyr for the past million years and ± 6 kyr for the interval from 1.0 to 1.5 Ma (Lisiecki and Raymo, 2005).

The chronology used in this paper is a hybrid model constructed using a combination of age-depth points from MD01-2444 and U1385. The age model is accurate to a precession cycle (~ 23 kyrs) but cannot provide exact absolute or relative dates for millennial events. This shortcoming limits the reliability of suborbital spectral peaks and estimation of recurrence times of millennial events. Nonetheless, the relative phasing of signals recording different components of the ocean-atmosphere system can be determined stratigraphically without the need for a time scale that is accurate at suborbital resolution. This is particularly important for inferring the phase relationship between planktic and benthic $\delta^{18}\text{O}$, which reflects the interhemispheric leads and lags of the two polar regions.



3. Results

3.1 Defining millennial variability

To identify millennial events, it is necessary to isolate the high-frequency component of the record by eliminating the low-frequency variations related to direct orbital forcing. We experimented with several methods for accomplishing this task including high-pass filtering, Gaussian smoothing of the record followed by calculation of a residual, and subtracting the planktic and benthic $\delta^{18}\text{O}$ values from one another. Although there are subtle differences in detection of millennial events depending on the method and thresholds used, the fundamental identification of millennial events was similar among methods. For simplicity, we settled on a high-pass Butterworth filter of second order with a cutoff frequency starting at 1/20 ky. The data were interpolated to equal time steps of 0.2 ka prior to filtering.

We identified stadial and interstadial events using the ‘findpeaks’ function in MatLab by specifying a peak height that must exceed a threshold defined by a multiplier of the standard deviation of the data (e.g., 1σ or 1.5σ), and a minimum peak duration and recurrence time (1 kyr). We varied the parameters so that the algorithm correctly identifies all known D-O events for the last glacial cycle in Core MD01-2444. The same parameters are then applied to identify millennial events for the entire length of the record.

There is some degree of subjectivity involved in identifying millennial events. If the same event is identified in both the planktic $\delta^{18}\text{O}$ and Zr/Sr signals (Figs. 4 and 5), we can be confident the event is robust; however, this is not always the case. Not every millennial event in planktic $\delta^{18}\text{O}$ has a corresponding change in Zr/Sr, which preferentially records the strongest of the stadial events. Additionally, the planktic $\delta^{18}\text{O}$ record can miss stadial events associated with glacial terminations (i.e., terminal stadial event) because the decrease in the $\delta^{18}\text{O}$ of seawater from melting ice overwhelms the $\delta^{18}\text{O}$ increase expected from cooling. In this case, we rely on the increase in Zr/Sr to recognize the event. Most terminal stadial events are also associated with a minimum in benthic $\delta^{13}\text{C}$ that can be used as an ancillary indicator of these events near glacial terminations. Forthcoming high-resolution measurements of the alkenone SST proxy at Site U1385 will greatly improve the identification of millennial events, especially those associated with terminations (Rodrigues et al., 2017).



We summed the number of millennial events (stadials + interstadials) over a moving non-overlapping window of 10-kyr for both planktic $\delta^{18}\text{O}$ and Zr/Sr. Patterns of millennial variability were similar for the two proxies (Figs 4 and 5). The number of events per 10-kyr interval changes depending upon the choice of start time of the 10-kyr window and whether the analysis is run forward or backwards, but the fundamental patterns are not substantially altered. The greatest number of millennial events per 10-kyr interval occurred during MIS 3 and glacial stages of the early Pleistocene from MIS 38 to 46.

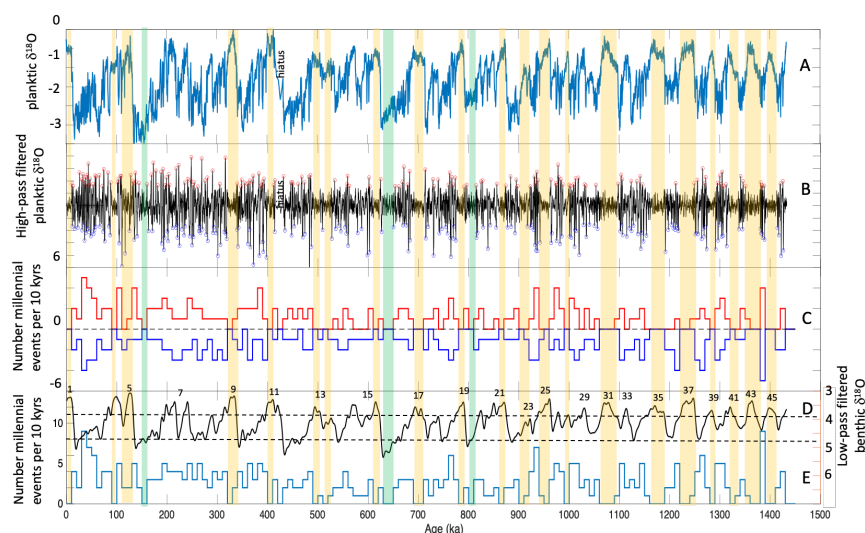


Figure 4. (A) The $\delta^{18}\text{O}$ record of *G. bulloides* at Site U1385. (B) High-pass filter of (A) to remove orbital frequencies and extract suborbital variability. Stadial (blue circles) and interstadial (red circles) events are identified by values that are greater than 1 standard deviation from the mean. (C) The number of stadial (blue) and interstadial (red) events in non-overlapping windows of 10,000-year duration. (D) Low-pass filter of benthic $\delta^{18}\text{O}$ record (black) used to lookup $\delta^{18}\text{O}$ values for each millennial event. Horizontal dashed black lines correspond to the benthic $\delta^{18}\text{O}$ thresholds marking the window of enhanced millennial variability. (E) The number of millennial events is the sum of the stadial and interstadial events in (C). The orange shade indicates times when there are no millennial events per 10,000 years associated with full interglacial stages. Green shade indicates where there are no millennial events per 10,000 years associated with full glacial stages.

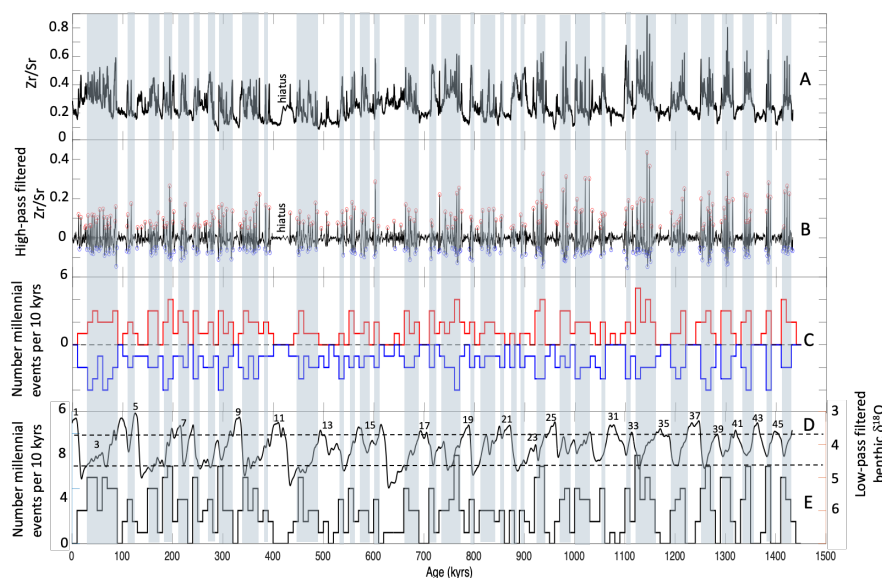


Figure 5. Same as Figure 4 but for Zr/Sr. The blue shade indicates times when the total number of millennial events equals or exceeds 3 per 10,000 years, which occurs mostly during intermediate glacial states.

3.2 Power Spectra

Time series analysis was performed using Acycle (Li et al., 2019) in the MatLab environment. The power spectra of planktic $\delta^{18}\text{O}$ and Zr/Sr show significant peaks at ~ 100 ka, 41 ka and 23 ka in the orbital band (Fig. 6). The suborbital part of the spectrum is complex with many high-frequency peaks. The spread of frequencies may partly reflect error associated with the chronology that smears the concentrations of any spectral energy across a wide band of frequencies (Rhines and Huybers, 2011). We have more confidence in spectral peaks that occur in both isotopic and lithologic records but spectral estimates are highly susceptible to sedimentation rate changes and age model errors. We recognize a band of peaks between 4 and 6 kyrs and many peaks with periods less than 3 kyrs. This is generally consistent with observations of a grouping of millennial events for MIS 3 into those with longer (Bond cycles) and shorter (D-O events) recurrence times.

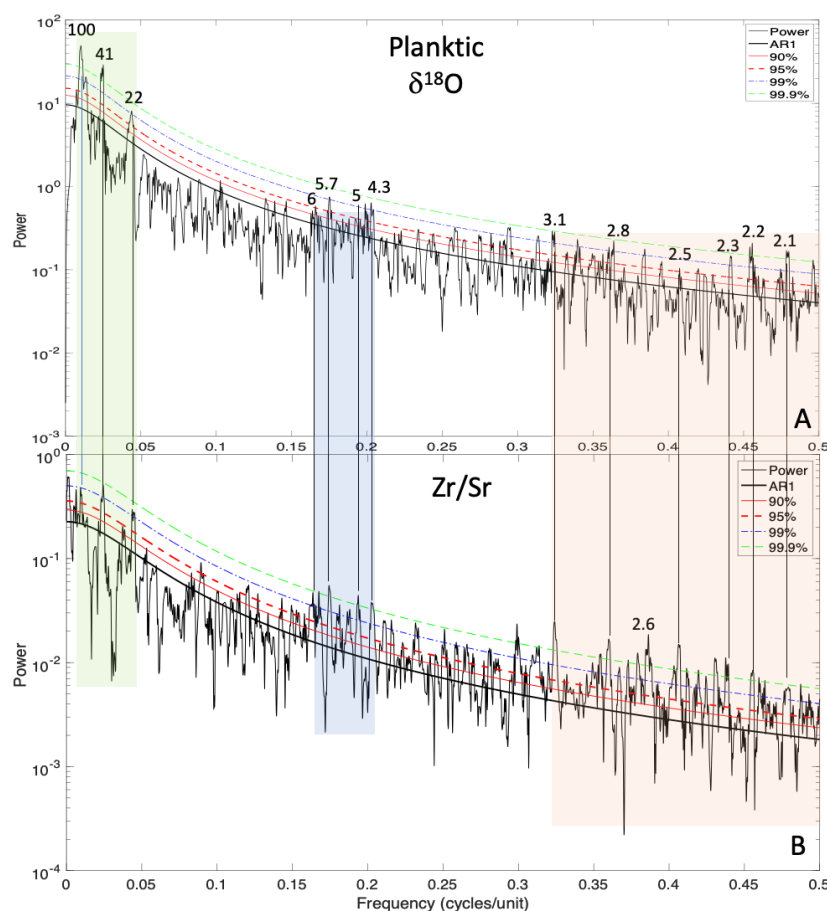


Figure 6. Spectral analysis of planktic $\delta^{18}\text{O}$ of *G. bulloides* (A) and Zr/Sr (B) using the multitaper method. Significant peaks shared between the two spectra are labeled with corresponding periods in kyr. Orbital bands are highlighted in green. A cluster of peaks occur between 6 and 4 kyr (blue shade) and the remainder <3 kyr (red shade).

3.3 Description of records

Because it is difficult to distinguish millennial events when the Site U1385 record is plotted full scale (Fig. 3), we describe the time evolution of orbital and suborbital variability in the isotope and XRF records for the last 1.45 Ma in ~200-kyr increments: 0-200 ka (Fig. 7); 200-400 ka (Fig. 8); 400-600 ka (Fig. 9); 600-800 ka (Fig. 10); 800-1000 ka (Fig. 11); 1000-1200 ka (Fig. 12); 1200-1450 (Fig. 13). We begin with the last 200 kyr because this is the best known period for MCV that can be used as a benchmark for comparison with MCV in the older



intervals. Within each interval the record is described oldest to youngest. The records consist of planktic $\delta^{18}\text{O}$, benthic $\delta^{18}\text{O}$, benthic $\delta^{13}\text{C}$ and Zr/Sr with stadial events identified by the gray shading. We use a modified version of the isotope nomenclature of Railsback et al. (2015) for marine isotope stages (MIS) of the last million years and the detrital layer stratigraphy of Channell et al. (2012) for Heinrich events.

3.3.1 MIS 1-7a (0-200 ka)

The interval from 0 to 200 ka consists mainly of the record of MD01-2444 which has been described in previous publications (Martrat et al., 2007; Margari et al., 2010, 2014; Hodell et al., 2013). MIS 6 shows a typical pattern of strong MCV at the time of glacial inception following MIS 7a (Fig. 7). Six millennial events are recognized between ~195 and 155 ka with a recurrence time ranging from 3 to 7 kyrs (Margari et al., 2010, 2014), which also correspond with carbon dioxide maxima (Shin et al., 2020). Minimum benthic $\delta^{13}\text{C}$ values occur at ~155 ka during event 6vi, which is associated with very cold alkenone SSTs (Margari et al., 2014). MCV becomes more subdued during the full glacial conditions of MIS 6 following by Heinrich stadial 11 associated with Termination II. MIS 6 shows a clear pattern of decreasing MCV during the glacial cycle with suppressed variability at the time of peak glaciation. Loulergue et al (2008) using ice core methane and Antarctic $\delta^{18}\text{O}$ showed a similar pattern of millennial variability, with 5 interstadial events identified between 190 and 170 ka but only 1 event between 170 and 140 ka. These patterns are also reflected in marine oxygenation reconstructions from the Southern Ocean (Gottschalk et al., 2020). The close similarity in pattern between planktic $\delta^{18}\text{O}$ and methane, and between benthic and Antarctic ice $\delta^{18}\text{O}$, continues throughout the record (Wolff et al., 2022).

Low-amplitude MCV occurs during MIS 5e (Tzedakis et al., 2018) and is followed by three strong stadial events during MIS 5d. MIS 5b is marked by a single prolonged period of stadial conditions. Millennial events DO 20 and 21, documented in the Greenland ice core, are recorded on the transition from MIS 5a to 4. MCV was relatively suppressed during MIS4 except for a single event (DO 18). The last glacial cycle is unusual in that it is interrupted by a long period of strong millennial variability during MIS 3 followed by a decreased amplitude during the last glacial maximum (MIS 2) between ~27 and 19 ka (Fig. 2). MIS 2 is terminated beginning with Heinrich stadial 1 which marks the start of deglaciation. Termination I includes millennial events that occurred during the deglaciation including the Bølling-Allerød interstadial and Younger Dryas stadial.

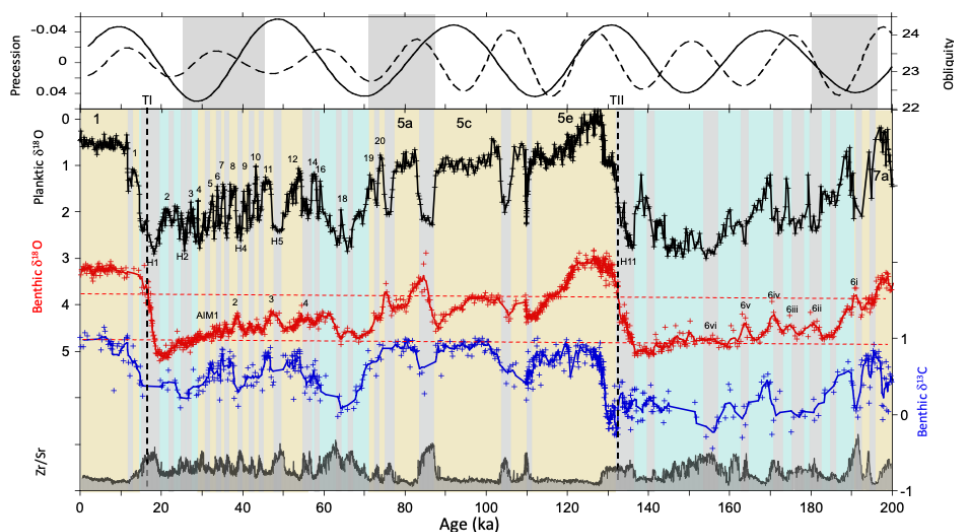


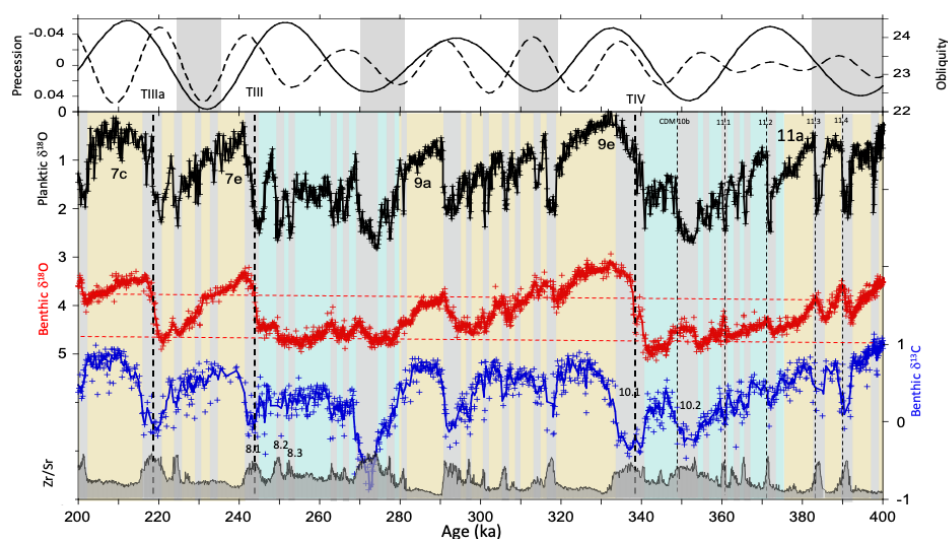
Figure 7. 0–200 ka: Planktic $\delta^{18}\text{O}$ of *G. bulloides* (black), benthic $\delta^{18}\text{O}$ of *Cibicidoides spp* (red), obliquity (solid line), precession (dashed line), benthic $\delta^{13}\text{C}$ of *C. wuellerstorfi* (blue), and Zr/Sr (gray). Odd marine isotope stages are numbered and shaded yellow. Glacial periods are shaded blue with stadial events identified by gray vertical bars. Stadials during MIS 6 are numbered after Margari et al. (2010). Terminations are indicated by vertical dashed black lines and roman numerals have been placed approximately near the mid-point of the deglaciation although millennial events on the termination often make it difficult to exactly define this point. Horizontal dashed red lines correspond to the benthic $\delta^{18}\text{O}$ thresholds marking the window of enhanced millennial variability. Precession and obliquity are plotted such that boreal summer insolation increases in the up direction. The gray shading indicates times when strong MCV is associated with declining or low obliquity, especially associated with glacial inception.

3.3.2 MIS 7c–11 (200–400 ka)

The transition from MIS 11 to 10 was marked by strong MCV (Fig. 8) and features in planktic and benthic $\delta^{18}\text{O}$ at Site U1385 can be readily correlated to the EPICA ice core records of methane and δD , respectively (Nehrbass-Ahles et al., 2020). Initially, the events are paced ~5 kyr apart from 400 to 370 ka and the recurrence time decreases to ~3 kyrs between 365 and 355 ka. MIS 10 culminates in two prolonged Heinrich stadials (10.1 and 10.2) before Termination IV. Low benthic $\delta^{13}\text{C}$ values ($<0\text{‰}$) occur at 338 and 352 ka associated with HS 10.1 and 10.2. MCV is muted during MIS 9a and 9e but relatively strong in the period between 9a and 9e. MCV resumes during MIS 8 including three Heinrich stadial events (8.1, 8.2, 8.3)



473 prior to Termination III. Minimum $\delta^{13}\text{C}$ values during MIS 8 occur at 272 ka associated with
 474 a very strong cooling event in alkenone SST (Rodrigues et al., 2017). MCV occurs on the
 475 transition from MIS 7e to 7d and is relatively suppressed during MIS 7c.
 476
 477
 478



479
 480 **Figure 8.** Same as Fig. 7 but for 200-400 ka.

481 482 3.3.3 MIS 11c-15c (400-600 ka)

483
 484 Both MIS 15d and 15b contain two strong stadial events, whereas MCV was suppressed during
 485 15a, c and e (Fig. 9). MIS 14 was a relatively weak glacial by late Pleistocene standards and
 486 MCV occurred throughout most of the glacial, and especially on the MIS 15a/14 transition.
 487 MIS 13 shows relatively low variability with one stadial event in 13c and two near the 13b/a
 488 transition. Strong MCV is recorded on the glacial inception of MIS 12 followed by a trend of
 489 declining amplitude towards the peak of MIS12. A minimum in benthic $\delta^{13}\text{C}$ values of $<0\text{‰}$
 490 occurs in the middle of MIS 12 at 455 ka. A short hiatus (~30 kyr duration) occurs at the
 491 transition from MIS 12 to 11 that removed much of Termination V and early MIS 11.

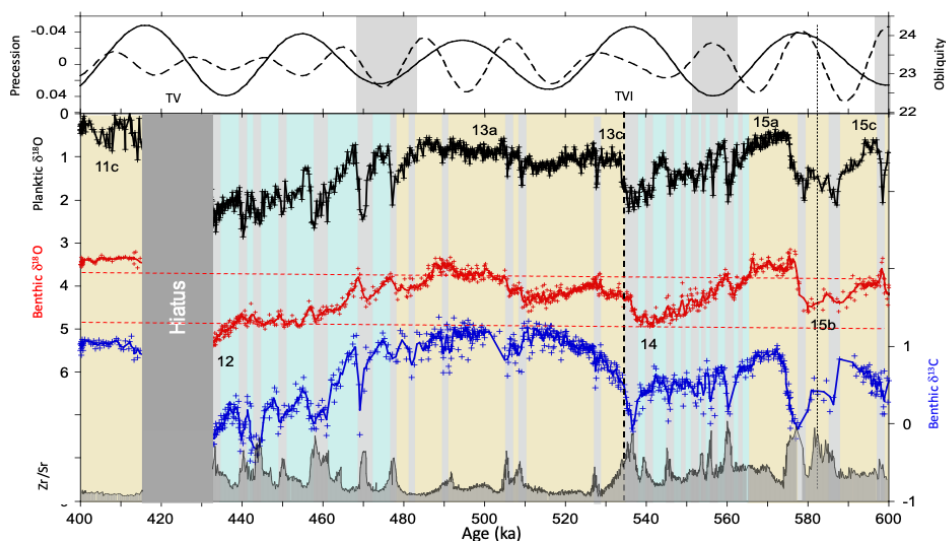


Figure 9. Same as Fig. 7 but for 400-600 ka.

3.3.4 MIS 15e-20 (600-800 ka)

The end of MIS 20 is marked by a terminal stadial event and decrease in benthic $\delta^{13}\text{C}$ at 795 ka (Fig. 10). Following MIS 19, strong MCV occurs on the MIS 19/18 transition with three distinct millennial oscillations paced at ~ 5 kyrs, which have been interpreted to reflect the second harmonic of precession (Ferretti et al., 2015; Sanchez-Goni et al., 2016). MIS 19 is the oldest interglacial recorded in the EPICA Dome C (EDC) ice core and three consecutive warming events (AIM) occur on the MIS 19/18 transition (Jouzel et al., 2007; Pol et al., 2010), which were also identified in the CH_4 and CO_2 signals (Loulergue et al., 2008; Lüthi et al., 2008). At Site U1385, the phasing between planktic and benthic $\delta^{18}\text{O}$ variations during the MCV on the MIS19/18 transition is similar to that observed during MIS 3, suggesting an active bipolar seesaw (Fig. 2). The phasing between methane and δD in the EPICA ice core is difficult to determine because of large uncertainties in gas age-ice age offsets and possible diffusion in the deepest part of the ice core.

MIS 18 consists of two distinct glaciations separated by a long interstadial period that is punctuated by a stadial event in the middle at 730 ka. Millennial variability decreases throughout the glacial inception towards the first glacial peak associated with a decrease in benthic $\delta^{13}\text{C}$ at 742 ka. The second glacial peak of MIS 18 is marked by a very strong decrease in benthic carbon isotope values at 717 ka associated with Terminations VIIIA.



MIS 16 shows a trend of decreasing amplitude of MCV through the glacial cycle where the variability is greatest on the MIS 17/16 glacial transition and diminishes towards the peak glacial conditions of MIS 16. Strong stadial events associated with Heinrich events 16.1 and 16.2 are suspiciously absent near Termination VII, perhaps indicating the presence of a previously undetected hiatus.

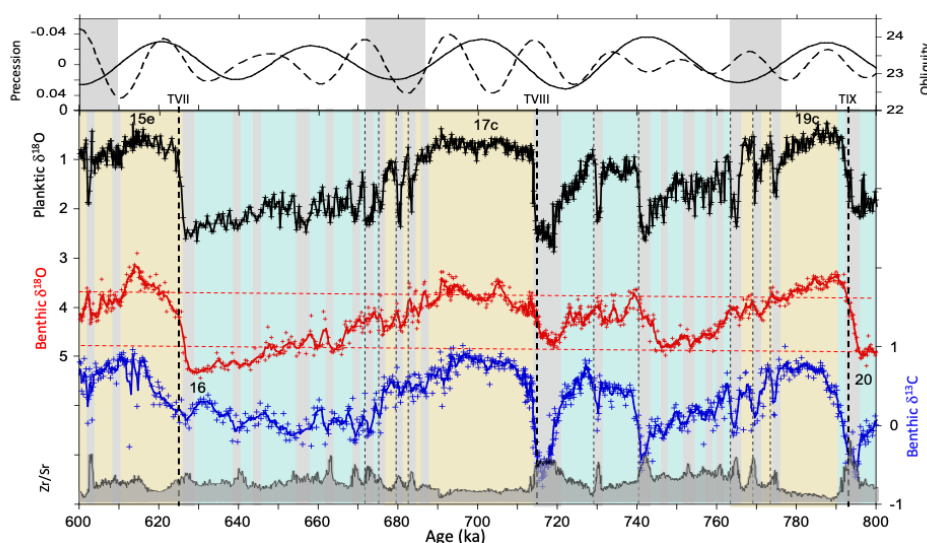


Figure 10. Same as Fig. 7 but for 600-800 ka.

3.3.5 MIS 21-27 (800-1000 ka)

The pattern of increased MCV associated with the transitions from interglacial to glacial stages continues with MIS 27/26 (Fig. 11). MIS 26 and 28 were relatively weak glacials and marked by strong millennial variability. The interval from MIS 25-21 is often compared with MIS 5-1 because of the similarity of weak interglacial MIS 23 to MIS 3. MIS 25-21 is sometimes erroneously described as the first ‘100-kyr cycle’, but it consists of two obliquity cycles (Bajo et al., 2020). The MIS 24/23 transition (TXI) was an incomplete (skipped) deglaciation, thereby lengthening the duration of glacial conditions to ~80 kys. The pace of millennial events is faster on the MIS25/24 transition than for some other glacial inceptions. Strong MCV is evident throughout MIS 24 and, unlike MIS 3, MCV is relatively suppressed during MIS 23, which contains a single strong millennial event at 919 ka. This pattern is different from the last glacial cycle when MCV was suppressed during MIS 4 and enhanced during a significant portion of MIS 3.

Glacial ice volume increased (Elderfield et al., 2012) during MIS 25-21 and major changes occurred in deep-ocean circulation (Pena and Goldstein, 2014) and carbon cycling (Thomas



and Hodell, in press). Minimum benthic $\delta^{13}\text{C}$ values occurred at 878, 898, and 925 ka, which are among some of the lowest values found in the deep North Atlantic during the Quaternary (Raymo et al., 1997; Hodell and Channell, 2016). MIS 21 has multiple substages and consists of four warm periods that are spaced about 10 kyrs apart, which have been interpreted as the second harmonic of precession (Ferretti et al., 2010).

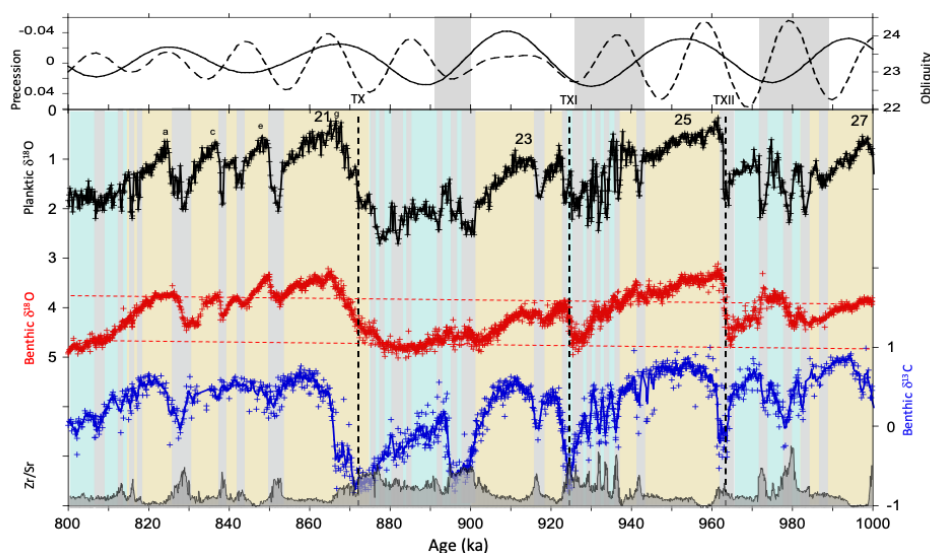


Figure 11. Same as Fig. 7 but for 600-1000 ka.

3.3.6 MIS 28-36 (1000-1200 ka)

The start of the MPT occurred at 1200 ka (Clark et al., 2006). From 1200 ka onward, the length of some of the glacial-interglacial cycles increase and the shape of the $\delta^{18}\text{O}$ signal becomes less symmetrical and takes on a decidedly more sawtooth waveform (Broecker and van Donk, 1970), reflecting a slower rate of ice sheet growth and faster rate of decay.

MIS 35-34-33 has a different duration and shape than previous glacial cycles -- it is drawn out with ~90 kyrs between TXVI and TXIV. MIS 35 was an exceptionally long interglacial (Shackleton et al., 1990). Very strong MCV occurred on the MIS 35/34 transition (Fig. 12), consisting of four prominent events that are paced about 5-6 kyrs apart. The abrupt warming events that mark the start of interstadials coincide with minima in benthic $\delta^{18}\text{O}$, indicating that the phase relationship is similar to that observed during MIS 3 between Greenland and Antarctica (Fig. 2), which is a pattern indicative of the bipolar seesaw. The benthic $\delta^{13}\text{C}$ mirrors the planktic $\delta^{18}\text{O}$ record with strong decreases in benthic $\delta^{13}\text{C}$ associated with each of the stadial events.



The stadial events become progressively colder during MIS 34 culminating in the terminal stadial event that occurs near the MIS 34/33 transition (TXV). This stadial is marked by a strong decrease in benthic $\delta^{13}\text{C}$. Benthic $\delta^{18}\text{O}$ begins to decrease first while planktic $\delta^{18}\text{O}$ remains high (cold) and benthic $\delta^{13}\text{C}$ low. This is the same phasing as observed during Termination I on the Iberian margin when the Southern Hemisphere begins to warm at ~ 18 ka as the North Atlantic remains cold and NADW shoals (Skinner and Shackleton, 2006).

Millennial events occur within MIS 33 and on the glacial inception of MIS 32 with a strong terminal stadial event associated with MIS 32/31 (TXIV). MIS 31 (1094–1062 ka) was also a relatively long and strong interglacial (Oliveira et al., 2017). MCV occurs on the 33/32, 31/30 and 29/28 glacial inceptions and each is associated with declining obliquity.

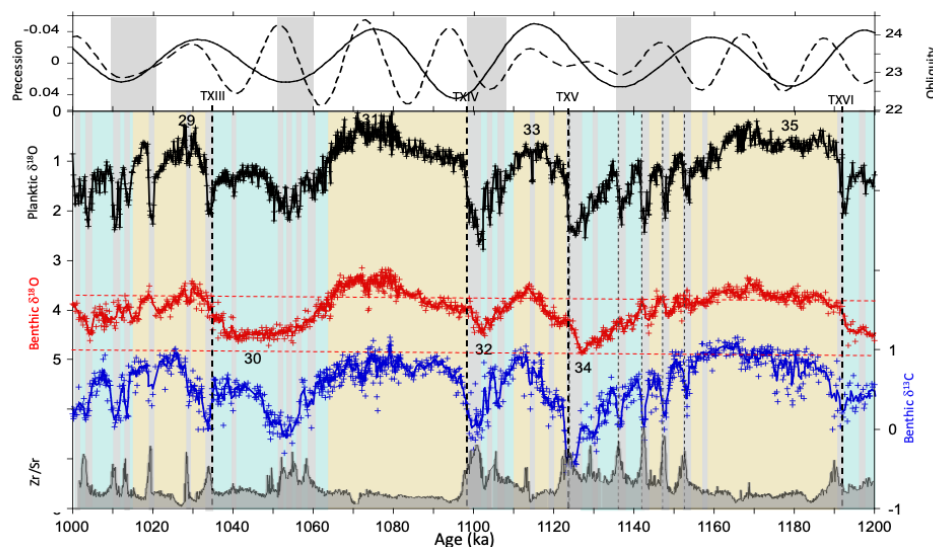


Figure 12. Same as Fig. 7 but for 1000–1200 ka.

3.3.7 MIS 37–47 (1200–1440 ka)

The period from ~ 1250 to 1550 ka (MIS 52) in the early Pleistocene was a time when glacial/interglacial cycles varied dominantly at a 41-kyr period coinciding with variations in Earth's obliquity, although precession was still significant (Liautaud et al., 2020). Similar to the last glaciation and Holocene, MCV is enhanced during glacial periods and suppressed during interglacial stages, exhibiting a threshold response (Fig. 13). MCV increases when obliquity drops below a threshold value of 23.5° , which corresponds to a benthic $\delta^{18}\text{O}$ threshold of $\sim 3.8\text{‰}$ (corrected to *Uvigerina*). Importantly, and unlike late Pleistocene glaciations after



the MPT, MCV persists throughout most of the glacial part of the cycle. Many of the increases in planktic $\delta^{18}\text{O}$ (stadial events) are associated with coeval decreases in benthic $\delta^{13}\text{C}$ indicating a link between North Atlantic surface climate and deep-water circulation.

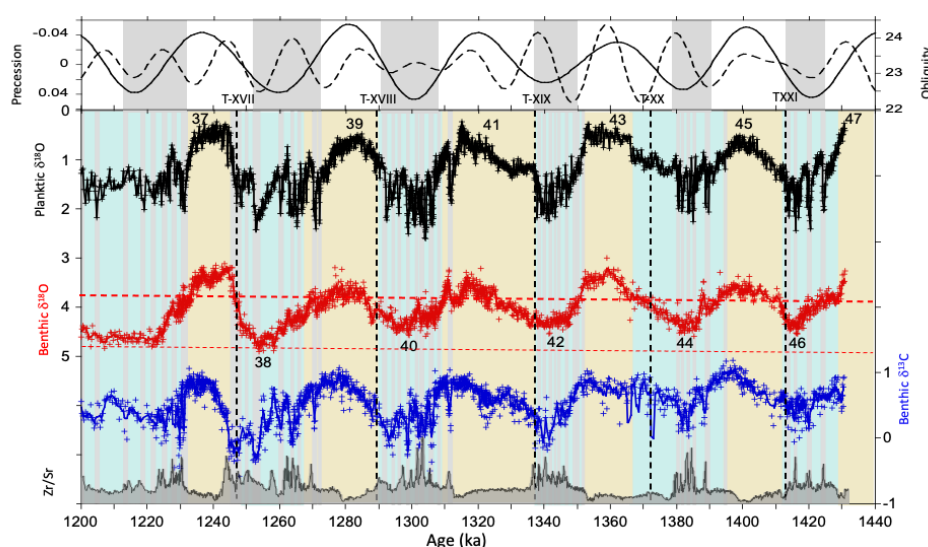


Figure 13. Same as Fig. 7 but for 1200-1440 ka.

4. Discussion

4.1 Millennial variability in planktic $\delta^{18}\text{O}$

Because of the great similarity between Greenland $\delta^{18}\text{O}$ and Iberian margin planktic $\delta^{18}\text{O}$ signals for the last glacial cycle, we interpret this proxy of surface temperature as an indicator of MCV in the North Atlantic. XRF records of Site U1385 provided the first evidence that MCV was a persistent feature of the climate system for at least the past 1.45 Ma (Hodell et al., 2015), which is confirmed by comparison of the planktic $\delta^{18}\text{O}$ and Zr/Sr signals (Figs. 4 and 5). The first-order pattern is that MCV is enhanced during glacial stages and diminished during each of the full interglacial stages (see shading in Fig. 4), which is consistent with the relative stability of Holocene climate relative to the last glacial period in the Greenland ice core and with other paleoclimatic results (McManus et al., 1999; Barker et al., 2021; Sun et al., 2021; Kawamura et al., 2017). A repeated pattern is that the end of each interglacial stage is marked by the onset of strong MCV that continues through the period of glacial inception when ice sheets are expanding on North America and Eurasia. MCV associated with glacial inceptions have generally longer recurrence times than D-O events varying between 3 and 8 kyrs. A few



glacial cycles of the late Pleistocene show a clear pattern of decreasing amplitude of MCV from the glacial inception towards peak glacial conditions (e.g., MIS 6, 10, 12, and 16, Figs 7-10), giving rise to a saw-tooth shape. The pattern of MCV evolves from longer stronger interstadials to shorter weaker interstadials as climate becomes progressively cooler during the glacial cycle. It is the MCV that constitute the unevenly-spaced teeth in the saw-tooth pattern if you will. The last glacial cycle is unusual in that the low MCV during MIS 2 and 4 is interrupted by a period of strong variability during MIS 3. Such D-O-type MCV has a short recurrence time (1.5-2 kyrs) which is also found during early Pleistocene glaciations prior to 1.25 Ma (Birner et al., 2016). Almost all glacial periods end with a strong terminal stadial event that marks the start of deglaciation with some terminations containing additional millennial events during deglaciation (e.g., Bolling-Allerod and Younger Dryas oscillations).

4.2 Millennial variability in benthic $\delta^{18}\text{O}$

Unlike planktic $\delta^{18}\text{O}$, Shackleton et al. (2000, 2004) demonstrated that variations in the benthic $\delta^{18}\text{O}$ signal of piston cores from the Iberian margin closely follows the δD record of Antarctic ice cores for the last glacial period (Fig. 2). The Site U1385 record indicates that this similarity extends for the last 800 ka (Fig. 14; Nehrbass-Ahles et al., 2020). The reason for the similarity of Iberian margin benthic $\delta^{18}\text{O}$ and Antarctic temperature is not entirely clear (Skinner et al., 2007). Shackleton et al. (2000) originally proposed the millennial oscillations in benthic $\delta^{18}\text{O}$ during MIS 3 reflected changes in the $\delta^{18}\text{O}$ of seawater caused by ice volume variations of the order of 20 - 30 m of sea level equivalence (Siddall et al., 2008). An alternative explanation is that millennial variations in benthic $\delta^{18}\text{O}$ reflect temperature changes of deep-water. In this case, the large variations in Antarctic air temperatures are damped by the thermal mass of the deep ocean and translate into small changes in benthic $\delta^{18}\text{O}$, reflecting temperature changes in the source areas of deep-water formation around Antarctica. The similarity of deep-water temperature estimated by Mg/Ca at ODP Site 1123 in the South Pacific and Antarctic temperature (Elderfield et al 2012) supports this interpretation, as does the emerging but sparse evidence for similarity between mean ocean temperature and Antarctic temperature (Haeberli et al., 2021). This interpretation implies that surface temperatures in the high-latitude Southern Ocean were important for regulating deep-ocean heat content, which has implications for deep ocean circulation and CO_2 storage (Jansen, 2018). Skinner et al. (2007) measured benthic Mg/Ca and $\delta^{18}\text{O}$ in core MD01-2444 during MIS 3 and concluded that the benthic $\delta^{18}\text{O}$ record cannot be interpreted as a unique proxy of either deep-water temperature or ice-volume and



must contain a significant local hydrographic component related to the mixing of end member water masses from the North Atlantic and Southern Ocean which have different $\delta^{18}\text{O}$ values. This is further supported by similar results from the deep Southern Ocean, where benthic $\delta^{18}\text{O}$ exhibits a similar (but not identical) pattern to that observed on the Iberian Margin (Gottschalk et al., 2020), and deep-water temperatures again appear to have decreased during HS4, consistent with enhanced convection contributing to Antarctic warmth and CO_2 rise (Skinner et al., 2020; Menviel et al., 2015). In all cases, a global glaciostatic signal would only be transported around the globe on a time-scale that is consistent with ocean transport and mixing (i.e. centuries to millennia) (Primeau and Deleersnijder, 2009), which would oppose any proposal of benthic $\delta^{18}\text{O}$ tracking global ice volume in synchrony (Gebbie et al., 2012). Indeed, this is demonstrated by the phasing of benthic $\delta^{18}\text{O}$, Antarctic temperature, mean ocean temperature, and sea level on the last deglaciation (Skinner et al., 2005; Baggenstos et al., 2019).

As in the latest Pleistocene, stadial events are associated with decreases in benthic $\delta^{13}\text{C}$ for the past 1.45 Ma, suggesting that surface coolings in the North Atlantic were associated with perturbations of deep-water ventilation and carbon storage in the deep-sea (Martrat et al., 2007; Shackleton et al., 2000; Skinner et al., 2007). Low $\delta^{13}\text{C}$ values are associated with each of the glacial terminations when $\delta^{18}\text{O}$ is decreasing and, in some cases, the low $\delta^{13}\text{C}$ values are prolonged and extend into the early part of the interglacial period (Hodell et al., 2009; Galaasen et al., 2014, 2020).

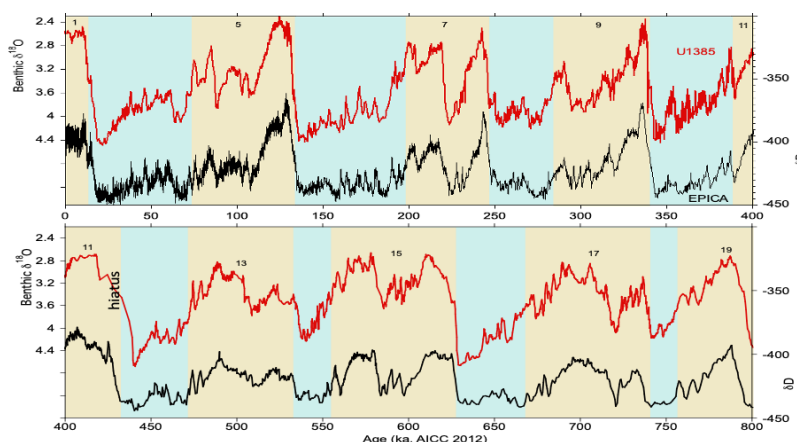


Figure 14. Comparison of benthic $\delta^{18}\text{O}$ from MD01-2444 and Site U1385 on the Iberian Margin and δD from EPICA Dome C ice core, Antarctica, for the last 800 kyrs.



4.3 Phasing of planktic and benthic $\delta^{18}\text{O}$ and the bipolar seesaw

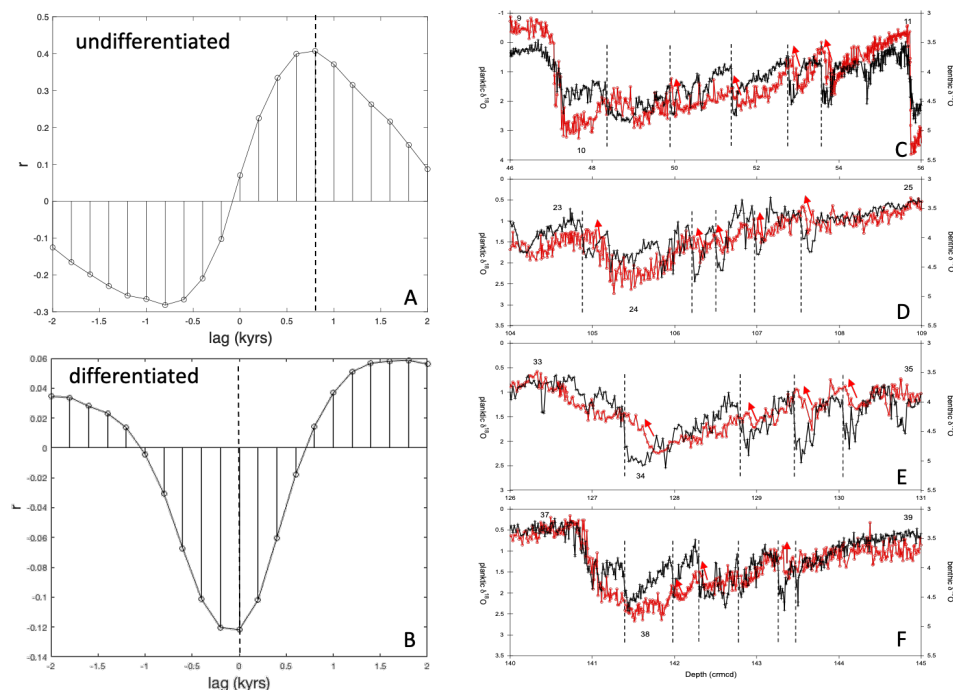
Because of the similarity of the planktic and benthic oxygen isotope records to Greenland and Antarctica, respectively, Shackleton et al. [2000] suggested the relative phasing of inter-hemispheric climate change could be assessed using a single core from the Iberian margin. To evaluate the phasing of MCV, oxygen isotope records of Site U1385 were first high-pass filtered to remove orbital-scale variability. Cross correlation analysis was then performed using the Matlab function xcorr. The filtered planktic and benthic $\delta^{18}\text{O}$ records are weakly correlated and show an average lead of ~ 0.8 ka for millennial variations in benthic $\delta^{18}\text{O}$ over those of planktic $\delta^{18}\text{O}$ for the past 1500 ka (Fig 15A). The lead of benthic over planktic $\delta^{18}\text{O}$ for the complete record is the same as that observed over shorter time intervals in piston cores during MIS 3 (Shackleton et al., 2000; Skinner et al, 2007) and for Site U1385 during MIS 38 and 40 (Birner et al., 2016). A cross correlation analysis of the isotope records in the depth domain yields a similar result.

This apparent time lead of the benthic over the planktic $\delta^{18}\text{O}$ is more likely the consequence of the different shapes of the benthic (rectangular) and planktic (triangular) signals (Hinnov et al., 2002). Rather than a direct lead/lag relationship between the polar regions, the thermodynamic bipolar seesaw model predicts an anti-correlation between Greenland temperature and the rate of change of Antarctic temperature with the abrupt warmings in Greenland leading the Antarctic cooling onset by about 200 years (WAIS Divide Ice Core members, 2015). This is equivalent to an antiphase relationship between planktic $\delta^{18}\text{O}$ (Greenland temperature) and the time derivative of the benthic $\delta^{18}\text{O}$ signal (Antarctic temperature) from the Iberian margin (Stocker and Johnsen, 2003; Barker et al., 2011). Because taking the derivative of a variable signal can result in noise, the filtered benthic $\delta^{18}\text{O}$ was first smoothed with a 5-point running mean. Although the correlation is poor, the phase shift is as predicted from the thermal bipolar seesaw model (Fig. 15B).

The consistent phase relationships between planktic and benthic $\delta^{18}\text{O}$ during millennial events for the past 1.45 Ma suggest the oceanic bipolar see-saw was a robust feature of the interhemispheric climate system. This phasing is similar despite differences in climate background state; for example, the phasing is the same during glacial inception as it is during deglaciations and intermediate ice volume states. Millennial variation in the AMOC and



703 thermal bipolar seesaw represent mechanisms by which MCV can be propagated to the broader
 704 climate system.



705 **Figure 15.** (A) Cross correlation coefficient (r) of the filtered signals of planktic and benthic
 706 $\delta^{18}\text{O}$. Positive offsets denote a lead of benthic $\delta^{18}\text{O}$ over planktic $\delta^{18}\text{O}$ by 800 yrs. (B) Cross
 707 correlation of planktic $\delta^{18}\text{O}$ and the time derivative of smoothed and benthic $\delta^{18}\text{O}$. Selected
 708 examples of the phasing of millennial benthic and planktic $\delta^{18}\text{O}$ variability in depth domain:
 709 (C) MIS 9 -11; (D) MIS 23-25; (E) MIS 33-35; and (F) MIS 37-39. The vertical dashed lines
 710 mark the rapid warmings (decreases) in the planktic $\delta^{18}\text{O}$ record and the red arrows indicate
 711 decreases in benthic $\delta^{18}\text{O}$. In most cases, the decrease in benthic $\delta^{18}\text{O}$ occurs prior to the
 712 decrease in planktic $\delta^{18}\text{O}$, which is similar to the phasing observed during MIS 3 (Figure 2).

714 4.4 Orbital modulation of MCV

717 To test for amplitude modulation of millennial variability by orbital cycles, we follow the
 718 approach of Hinnov et al. (2002) who analyzed the MD95-2042 record for the last 100 kyr.
 719 We examine the power spectrum of the planktic $\delta^{18}\text{O}$ and Zr/Sr records after applying a Taner
 720 filter and Hilbert transform. Bandpass filtering was performed on evenly resampled (0.2 kyr)
 721 time series using a Taner filter centered on 0.55 ± 0.45 with a roll-off rate $= 1 \times 10^{12}$, which has

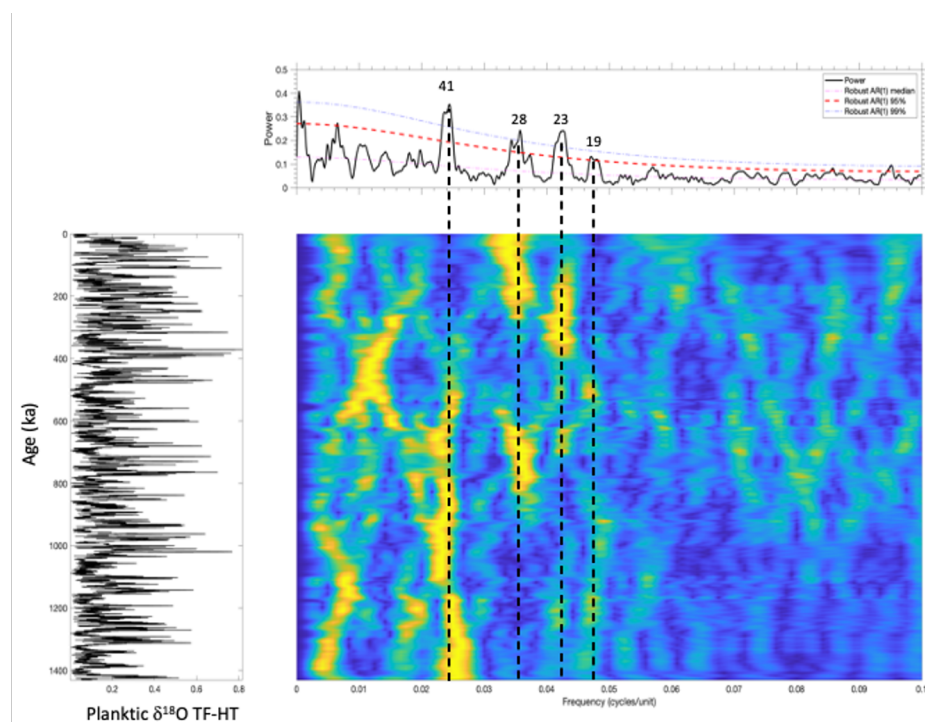


Figure 16. Evolutive power spectrum of the amplitude modulation of planktic $\delta^{18}\text{O}$ as estimated from a Taner filter (TF) centered at 0.55 ± 0.45 and Hilbert transformation (HT) of the time series. Sliding window of ~ 300 kyrs with time domain zero padding and a step equal to the sampling rate of the time series (~ 2 kyrs).

The power spectra of planktic $\delta^{18}\text{O}$ and Zr/Sr are similar and support orbital modulation of the amplitude of the millennial band by earth's orbital parameters (e.g., 19, 23, 28, 41 kyrs). The 41-kyr obliquity dominates the modulation of MCV between 1450 and ~ 900 ka with a weak precession component (Figs. 16 and 17). At ~ 900 ka, power develops at ~ 28 kyrs and precession strengthens, especially in the Zr/Sr record (Fig. 17). The 28-kyr cycle is a common feature of Pleistocene foraminiferal $\delta^{18}\text{O}$ records (Huybers and Wunsch, 2004; Lisiecki and Raymo, 2005; Lourens et al., 2010). The 28-kyr cycle has been interpreted as resulting from



non-linear interactions (combination tones) between eccentricity (quasi-100 kyrs) and precession (23 kyr) or obliquity (41 kyr). Lourens et al. (2010) suggested the 28-kyr cycle reflects the sum frequency of the primary 41-kyr cycle and its multiples (82 and 123 ky), and results from a non-linear response of the glacial cycles to obliquity forcing. At ~650 ka, the 41-kyr and 28-kyr power of obliquity decline substantially and the spectrum is marked by lower-frequency power (80-120 kyrs). This may reflect an increase in eccentricity modulation of MCV or modulation by multiples of the obliquity and precession cycles, or a change in the non-linear energy transfer between orbital components across the MPT (Liebrand and de Bakker, 2019).

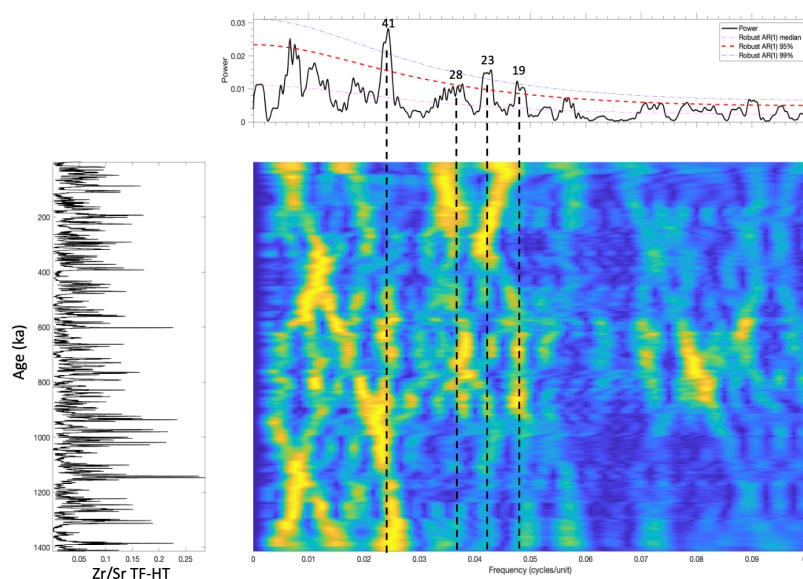


Figure 17. Same as Figure 16 but for Zr/Sr.

The early Pleistocene interval from 1200-1440 ka provides strong evidence for a relationship between the occurrence of MCV and obliquity (Fig. 13). MCV increases during times of low obliquity, displaying a threshold response such that it increases each time the obliquity drops below ~23.5°. It is uncertain, however, if the increased millennial variability is the direct (i.e., fast-acting) result of reduced insolation at high latitude caused by low obliquity (e.g., lowered insolation, colder temperature, sea ice expansion) or whether low obliquity secondarily leads to increased ice volume, ice-sheet height and lowered sea level (see Discussion section 4.5) --



759 all of which have been proposed as a threshold for MCV (McManus et al., 1999; Zhang et al.,
 760 2014).

761
 762 Some modelling experiments have demonstrated increased MCV during times of low obliquity
 763 in the absence of freshwater forcing (Friedrich et al., 2010; Brown and Galbraith, 2016;
 764 Galbraith and de Lavergne, 2018). The obliquity threshold observed for the early Pleistocene
 765 is highly suggestive of a non-linear system that is influenced by orbital cycles. For example,
 766 sea ice expansion during times of low obliquity may provide strong albedo-feedback
 767 amplification, resulting in a non-linear response (Tuentner et al., 2005). As the mean position of
 768 the sea ice edge expands to lower latitude, the region of deep water formation moves from the
 769 Norwegian-Greenland Sea to south of Iceland, shifting the AMOC with respect to the mean
 770 atmospheric precipitation field where precipitation exceeds evaporation, thereby making the
 771 system less stable (Sevellec and Fedorov, 2015, Friedrich et al., 2010).

772
 773 The relationship between low obliquity and enhanced MCV persists after 1.2 Ma and is
 774 expressed as increased millennial variability associated with the transitions from glacial to
 775 interglacial stages, which is always associated with declining obliquity (Tzedakis et al., 2012).
 776 In view of this, Tzedakis et al. (2012) proposed the end of interglacials could be defined as
 777 three thousand years (kyr) before the reactivation of MCV at the time of glacial inception. Low
 778 obliquity is important for controlling ice accumulation at the start of a glaciation because ice
 779 growth begins at high latitudes (and altitudes) where the effect of obliquity on summer
 780 insolation is strongest (Vettoretti and Peltier, 2004). Lower obliquity decreases the summer
 781 insolation at high latitudes, reduces seasonality and strengthens the insolation gradient between
 782 low and high latitudes, thereby increasing the meridional heat and moisture flux to the high
 783 latitudes (Mantis, 2011). The increased heat transport does not balance the direct cooling
 784 effects of obliquity through reduced insolation at high latitude. Increased moisture transport
 785 towards the poles provides the fuel needed for growing ice-sheets (Vimeux et al. 1999; Raymo
 786 and Nisancioglu 2003). The combination of reduced temperature and increased moisture flux
 787 are the two ingredients needed for rapid ice sheet growth during glacial inceptions. Precession
 788 and atmospheric CO₂ play secondary roles at glacial inceptions that may reinforce or delay
 789 increased ice accumulation depending on CO₂ concentration and the phasing of precession and
 790 obliquity (Vettoretti and Peltier, 2004).

791
 792 Modelling studies suggest that orbital forcing may play a more direct role in the onset of MCV
 793 at the end of interglacial periods. Using LOVECLIM1.3, Yin et al. (2021) found a threshold



response to decreasing summer insolation related to both precession and obliquity. When summer insolation falls below a critical value, a strong, abrupt weakening of AMOC is triggered as sea ice expands in the Nordic and Labrador Seas. The transition into a cooler mean climate state is accompanied by high-amplitude temperature variations lasting for several thousand years (Yin et al., 2021).

Zhang et al. (2021) used a fully coupled climate model and found that changes in Earth's orbital geometry can directly affect MCV during intermediate glacial states (e.g., MIS 3). Both obliquity and precession play a role in AMOC stability (Zhang et al., 2021; Yin et al., 2021) - obliquity through its effect on mean insolation at high latitudes and eccentricity-modulated precession through its low-latitude effect on the subtropical hydrologic budget and salinity of the North Atlantic basin.

MCV can also result from orbital forcing that is expressed as subharmonics and combination tones of the primary orbital cycles. Using bispectral analysis, Hagelberg et al. (1994) demonstrated that approximately a third of the variability in the frequency band ranging from 1/15 to 1/2 kyr originates from the transfer of spectral energy from the lower-frequency Milankovitch band (see also Liebrand and de Bakker, 2019). A case in point is the 11- and 5.5-kyr cycles found in MIS 21 and 19, respectively, that have been attributed to the second and fourth harmonics of the primary precession cycles (Ferretti et al., 2015; Sanchez-Goni et al., 2016). Berger et al. (2006) suggested the double maximum that occurs in daily irradiation at tropical latitudes includes a suborbital insolation forcing at 11-kyr and 5.5-kyr periods related to precession harmonics. Zhang et al. (2021) proposed a physical mechanism for MCV related to the effect of eccentricity-modulated precession through its low-latitude effect on the subtropical hydrologic budget and salinity of the North Atlantic basin.

4.5 State dependence of MCV

Orbital changes may influence MCV directly through fast processes (e.g., sea ice) or more indirectly through slow changes in ice sheet configuration (volume or height) and sea level. On the basis of a 500-ka-long record of ice-rafted detritus and summer SST from Site 980 at 55 °N in the Rockall Trough, McManus et al. (1999) suggested that MCV was enhanced during times of intermediate ice volume as defined by a window or "sweet spot" when MCV was most active during times of intermediate glacial states (Sima et al., 2004; Galbraith and de Lavergne, 2018). MCV is suppressed under full interglacial conditions and during some peak glaciations. The



concept of increased MCV during times of intermediate ice volume is supported by observations from the last glacial cycle when MCV was relatively suppressed during MIS 2 and 4 and strong during MIS 3. MCV was also frequent during glacial periods of the early Pleistocene between 1.45 and 1.25 Ma when glacial benthic $\delta^{18}\text{O}$ values fell entirely within the millennial window (Fig. 5). After 1.25 Ma, the benthic $\delta^{18}\text{O}$ threshold is crossed slowly during glacial inceptions and more quickly at glacial terminations (Sima et al., 2004) with some, but not all, full glacial periods marked by reduced MCV.

We tested whether there is a statistically significant tendency for millennial events to occur within a certain range of benthic $\delta^{18}\text{O}$ values at Site U1385. The FindPeak algorithm in MatLab returns the age of each event identified, which is then used to lookup its corresponding benthic $\delta^{18}\text{O}$ value. The $\delta^{18}\text{O}$ values are concatenated to form a subpopulation of benthic $\delta^{18}\text{O}$ values corresponding to millennial events that is compared with the full population of benthic $\delta^{18}\text{O}$ values (Fig. 18A&B). A two-sample Kolmogorov-Smirnov (K-S) test is used to evaluate if the two populations are from the same or different continuous distributions and whether the tail of the millennial subpopulation distribution is smaller than the full population of benthic $\delta^{18}\text{O}$ values.

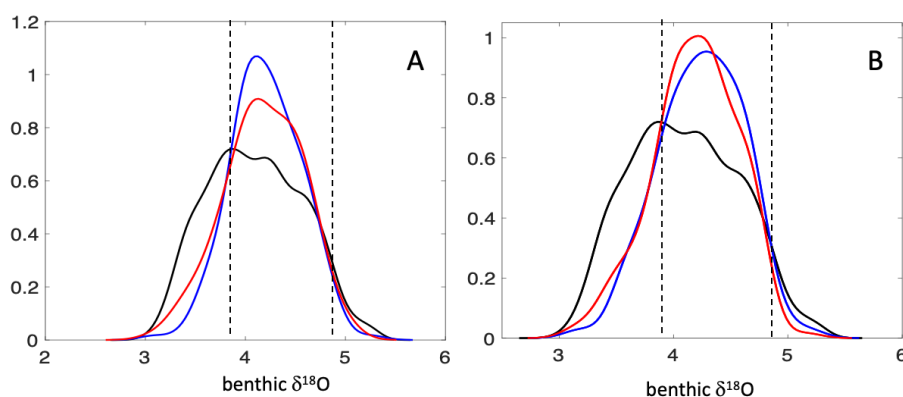


Figure 18. Probability density estimate of benthic $\delta^{18}\text{O}$ for all values (black), interstadial (red); and stadial (blue) events for planktic $\delta^{18}\text{O}$ (A) and Zr/Sr (B). Vertical dashed lines represent benthic $\delta^{18}\text{O}$ threshold values for MCV that define the millennial window.

For millennial events identified in both planktic $\delta^{18}\text{O}$ and Zr/Sr, the millennial benthic $\delta^{18}\text{O}$ population was significantly different from the full population at 95% confidence, and the tail of the millennial populations was significantly smaller than that of the full $\delta^{18}\text{O}$ population.



855 Millennial events are clearly less frequent at the low (warm) end of the benthic $\delta^{18}\text{O}$
 856 distribution suggesting reduced MCV during full interglacial periods. We estimate the lower
 857 benthic $\delta^{18}\text{O}$ threshold to be $\sim 3.8\text{‰}$ for both planktic $\delta^{18}\text{O}$ and Zr/Sr (note that 0.64‰ must
 858 be subtracted from this value to convert to the *Cibicidoides* scale) (Fig. 11C&D). The $\delta^{18}\text{O}$
 859 threshold for MCV may differ depending on the record and proxy used to identify millennial
 860 variability (IRD, SST, planktic $\delta^{18}\text{O}$, etc.) and may be non-stationary through time. For
 861 example, Bailey et al. (2010) suggested that the $\delta^{18}\text{O}$ threshold for the late Pliocene (MIS G4
 862 at ~ 2640 ka and MIS 100 at ~ 2520 ka) was 0.45‰ lower than that of the late Pleistocene. For
 863 the period 1240 to 1320 ka at Site U1385, Birner et al. (2016) suggested the threshold was
 864 3.2‰ on the *Cibicidoides* scale which is equivalent to 3.84‰ on the *Uvigerina* scale. This is
 865 the same value we have estimated for the entire 1.5 million yr interval, suggesting the benthic
 866 $\delta^{18}\text{O}$ threshold has not changed significantly at Site U1385. The existence of an upper $\delta^{18}\text{O}$
 867 threshold above which millennial variability is suppressed during peak glacial conditions is less
 868 clear from the probability density estimates (Fig. 18). However, several of the late Pleistocene
 869 glacial intervals (MIS 2, 4, 6, 10, 12, 16) show a pattern of strong MCV associated with glacial
 870 inception that decreases towards full glacial conditions ($>4.8\text{‰}$ on the *Uvigerina* scale),
 871 suggesting reduced MCV during maximal glacial conditions.

872
 873 The physical significance of the benthic $\delta^{18}\text{O}$ thresholds that define the millennial window is
 874 uncertain. Although several studies have suggested that MCV is related to ice volume, it's not
 875 certain which part of the climate-cryosphere system was responsible. Several processes have
 876 been suggested to trigger increased MCV including sea level dropping below a critical sill
 877 depth (e.g., Bering Sea; De Boer and Nof, 2004), the effect of ice sheet height on winds (Zhang
 878 et al., 2014), iceberg calving and freshwater fluxes to the oceans, or direct orbital forcing
 879 (Friedrich et al., 2010; Zhang et al., 2021; Yin et al., 2021).

880
 881 McManus et al. (1999) suggested that MCV was enhanced with a sea level lowering of as little
 882 as 30 m below modern. This may correspond to a critical sill depth such as the Bering Sea,
 883 which has a sill depth of ~ 45 m. De Boer and Nof (2004) proposed that the onset and cessation
 884 of flow through the Bering Strait was responsible for the switch between stable and unstable
 885 states of glacial versus interglacial climate. A restricted Bering Strait increases the sensitivity
 886 of AMOC to freshwater perturbation by blocking the escape route of freshwater to the Pacific
 887 via the Arctic (Poppelmeier et al., 2020; Hu et al., 2012a,b). Freshwater can accumulate in the



888 North Atlantic more readily with a closed Bering Strait, thereby increasing surface
889 stratification and leading to AMOC instability.

890

891 Because benthic $\delta^{18}\text{O}$ also depends on bottom temperature, the threshold could also be related
892 to surface temperature conditions in the source area of deep-water formation. For example, the
893 benthic $\delta^{18}\text{O}$ threshold could correspond to crossing the freezing point of seawater in deep-
894 water source areas in the North Atlantic, which would result in increased sea ice formation and
895 shift the region of deep-water formation to the south where the AMOC is more susceptible to
896 oscillation (Sevellec and Fedorov, 2015).

897

898 Galbraith and de Lavergne (2018) suggested that D-O-like variability in AMOC was more
899 likely to occur under a ‘sweet spot’ of interrelated conditions that included low obliquity, low
900 CO_2 and a low-elevation Laurentide ice sheet. By analyzing dust flux from the Dome Fuji ice
901 core (Antarctica) over the last 720 kys, Kawamura et al. (2017) also concluded that MCV was
902 more likely during times of intermediate glacial states. Because glacial climate state is
903 ultimately affected by orbital geometry, an inherent link must exist between climate variability
904 on orbital and suborbital time scales (see discussion in section 4.4).

905

906 **4.6 MCV across the Middle Pleistocene Transition**

907

908 The MPT occurred between ~1200 and 650 ka and involved an increase in global ice volume
909 as the dominant period of glacial-interglacial cycles shifted from 41 kyrs before 1200 ka to
910 quasi-100 kyrs after 650 ka (Clark et al., 2006). Some studies have suggested that MCV was
911 less frequent during the early Pleistocene and increased across the MPT as the size of Northern
912 Hemisphere ice sheets expanded (Larrasoana et al., 2003; Weirauch et al., 2008; Bolton et al.,
913 2010). Others have found evidence for equally strong millennial variability in the early
914 Pleistocene as the late Pleistocene (Raymo et al., 1998; McIntyre et al., 2001; Tzedakis et al.,
915 2015; Grützner and Higgins, 2010; Hodell et al., 2008; Birner et al., 2016). Still others have
916 suggested MCV (as represented by IRD events) was more frequent but less intense prior to 650
917 ka because the climate system spent more time in the millennial window during the early
918 Pleistocene (Hodell et al., 2008; Hodell and Channell, 2016) and rarely exceeded the upper
919 benthic $\delta^{18}\text{O}$ threshold before 650 ka.

920

921 The planktic $\delta^{18}\text{O}$ and Zr/Sr records of Site U1385 clearly demonstrate that MCV was strong
922 during glacial stages both before and after the MPT. The main difference across the MPT is



that whereas MCV persists throughout the glacial periods prior to 1200 ka, it is most prevalent on the transitions both into and out of glacial states (i.e., inceptions and terminations) and during times of sustained intermediate ice volume, such as MIS 3. Beginning at 650 ka (MIS 16) following the MPT, MCV is suppressed during some of the strongest glacial periods associated with the growth of oversized continental ice sheets, which Raymo (1997) refers to as "excess ice".

A change occurred in the orbital modulation of MCV across the MPT as expressed in changes in the evolutive spectra of the Taner filter-Hilbert transform of the Zr/Sr and planktic $\delta^{18}\text{O}$ (Figs. 10 and 11). Prior to ~900 ka, the amplitude modulation of MCV was dominated by 41-kyr obliquity. Obliquity continues to modulate the amplitude of MCV from 900 to 600 ka, but with an increase in precession and the addition of a possible combination tone (28 kyrs) of the 41-kyr cycle.

At the end of the MPT (~600 ka), the power of obliquity declines and the spectra become more complex with greater modulation at lower frequencies (e.g. 100 ± 20 kyrs). Hodell et al. (2008) noted a similar change in the amplitude modulation of the Si/Sr IRD proxy at Site U1308 in the central North Atlantic IRD belt when, at ~650 ka, the power of the 41-kyr obliquity cycle decreased and quasi-100-kyr power increased. Hodell and Channell (2016) also observed that millennial variability in the Si/Sr IRD proxy was proportional to the power in the precessional band, suggesting an amplitude modulation of MCV by precession. Precession plays a greater role in modulating the amplitude of MCV in the late Pleistocene, in agreement with its steady increase in importance throughout the Quaternary (Liautaud et al., 2020).

At 0.65 Ma, the development of massive ice sheets on North America (Batchelor et al., 2019) introduced a new type of MCV related to dynamic instability of the Laurentide Ice Sheet in the region of Hudson Strait, which was expressed by the occurrence of Heinrich layers in North Atlantic sediment beginning in MIS 16 (Hodell et al., 2008; Hodell and Channell, 2016). Heinrich events tend to occur late in the glacial cycle and are associated with glaciations of long duration (Hodell et al., 2008). They are distinct from background IRD events in their magnitude, frequency and duration, and their impact on the global climate system was more widespread (Marshall and Koutnik, 2006). MCV associated with late Pleistocene terminations after 0.65 Ma are closely related to freshwater fluxes from the decay of oversized ice sheets, which play an important role in the progression of glacial terminations (Wolff et al., 2009; Barker and Lohman, 2021).



4.7 Influence of MCV on glacial-interglacial cycles

Ice dynamics may be an effective mechanism for propagating high-frequency variability to longer, orbital timescales (Verbitsky et al., 2019). For example, Siddall et al. (2006) suggested that sustained ice-sheet growth through a glacial cycle requires the absence of MCV. Niu et al. (2019) proposed that the presence of strong MCV may prevent an ice sheet from reaching its maximum size owing to surface mass balance effects. If true, then sustained MCV throughout the glacial periods of the early Pleistocene may have prevented ice sheets from growing as large as their late Pleistocene counterparts. In contrast, strong MCV on glacial inception may have significantly slowed ice sheet development giving rise to the sawtooth shape of the late Pleistocene benthic $\delta^{18}\text{O}$ signal. Ice sheets could only reach their maximum size during the latter part of the glacial cycle once MCV was suppressed.

The exact cause-effect relationship between MCV and ice sheet size is difficult to ascertain. Did ice sheets grow larger in the late Pleistocene because MCV was suppressed or did large ice sheets lead to a suppression of MCV during full glacial conditions? In either case, orbital and millennial-scale variability cannot be considered separately from one another because they interact. Verbitsky et al. (2019) demonstrated that ice sheet non-linearity allows MCV to propagate upscale and influence ice-age dynamics. In addition, non-linear ice-flow dynamics can propagate downscale and affect the millennial part of the spectrum.

High-frequency MCV constitutes a source of noise on orbital time scales, which may enhance the phase-locking of the response of the climate system to orbital forcing (Hodell and Channell, 2016). The theory of stochastic resonance has long been considered as a possible mechanism to explain how the climate system can be synchronized with relatively weak orbital forcing (Benzi et al., 1982). The noise for stochastic resonance is often assumed to be random and white, but MCV provides a source of noise to the climate system whose amplitude varies with climate background state -- i.e., relatively noisy glacials and quiet interglacials. Such oscillations in noise amplitude may be relevant for stochastic or coherence resonance in which the signal-noise resonance is important for phase locking (Liu and Chao, 1998). For example, glacial-interglacial variations during the early Pleistocene may consist of a resonant system in which the intensity of millennial variability is responding to obliquity-controlled changes in climate background state and, in turn, changes in the amplitude of MCV may aid in phase locking the climate system to the obliquity period.



4.8 MCV and atmospheric CO₂ variations

Because nearly all the rapidly exchangeable carbon in the ocean-atmosphere system is contained in the deep ocean, atmospheric greenhouse gas variations in ice cores are intimately linked to carbon storage in the deep ocean. Variations in benthic carbon isotopes at Site U1385 demonstrate that the millennial changes in planktic $\delta^{18}\text{O}$ are not only a feature of surface climate on the Iberian margin, but are crucially linked with changes in deep-water ventilation. Decreases in benthic $\delta^{13}\text{C}$ are associated with increases in planktic $\delta^{18}\text{O}$, indicating reduced ventilation of the deep North Atlantic during cold stadial events. A relationship between atmospheric CO₂ and centennial-millennial events in the North Atlantic exists for the last glacialiation and deglaciation (Marcott et al., 2014; Bauska et al., 2021) as well as for older periods such as MIS 6 (Shin et al., 2020) and the MIS 11-10 transition (Nehrbass-Ahles et al., 2020).

We suggest MCV may be involved in setting the minimum CO₂ values attained during glacial periods. Millennial variability in AMOC provides a mechanism by which deep-sea CO₂ can be degassed to the atmosphere. When MCV was strong during MIS 3, CO₂ varied between 200 and 220 ppm and the lowest sustained CO₂ levels of 180-190 ppm were only achieved during MIS 2 when MCV was suppressed during peak glacial conditions. By analogy with MIS 3, the persistently strong MCV that occurred throughout the glacialiations of the early Pleistocene (1.45-1.25 Ma) may have prevented CO₂ from reaching values as low as those attained during the late Pleistocene because CO₂ was episodically released from the deep-sea reservoir during strong millennial-scale AMOC events. In the early Pleistocene, boron isotope reconstructions suggest that fluctuations in CO₂ varied in phase with obliquity and benthic $\delta^{18}\text{O}$ (Chalk et al., 2017; Dyez et al. 2018). The threshold-type behaviour of MCV during the 41-kyr cycles of the early Pleistocene may have served as an important mechanism for linking internal climate dynamics with external astronomical forcing by regulating carbon storage in the deep-sea.

Evidence from Site U1385 for an active oceanic thermal bipolar see-saw during most of the prominent stadials during glacials of the 41-kyr world (Birner et al. 2016) supports a similar mechanism of CO₂ degassing via the Southern Ocean as that in MIS 3. Although CO₂ records are fragmentary before 800 ka, there is evidence for elevated glacial CO₂ with minimum values of 220 ppm during glacial periods between 1 and 1.25 Ma during the early MPT (Yan et al.,



2019; Higgins et al. 2015; Chalk et al., 2017; Hönlisch et al, 2012), and glacial CO₂ values may have been higher still before 1.25 Ma (Yan et al., 2019; Martinez-Botí et al., 2015).

We have emphasized the role that MCV may play in setting atmospheric CO₂ concentrations but others have suggested that, in contrast, atmospheric CO₂ may have a controlling influence on millennial-scale climate oscillations (Zhang et al., 2017; Vettoretti et al., 2022). Using an Earth system model, Vettoretti et al. (2022) demonstrated that nonlinear self-sustained climate oscillations appear spontaneously within an intermediate window of glacial-level atmospheric CO₂ concentrations between ~190 and 225 ppm.

Conclusion

The recognition of MCV in Greenland ice cores in the early 1980s ushered in the study of paleoceanographic records at a resolution that is at least 10 times greater than previous orbital-scale studies. Although the initial focus was on the last deglaciation and MIS 3, several long records of MCV are beginning to emerge (Hodell et al., 2008; Hodell and Channell, 2016; Hodell et al., 2015; Barker et al., 2021, 2022), thereby providing an opportunity to document the long-term relationship of climate variability on orbital and millennial timescales and their interactions. Consistent with previous findings, the U1385 record demonstrates that MCV was a persistent feature of intermediate glacial climate states for the last 1.45 Ma, including the 41-kyr world of the early Pleistocene prior to the MPT.

During glacial periods from 1.45 to 1.25 Ma, the amplitude of MCV was strongly modulated by changes in Earth's obliquity and exhibited threshold behaviour typical of a non-linear system. Beginning at 1.2 Ma at the start of the MPT, MCV becomes more focused on glacial inception, terminations and periods of intermediate ice volume. One of the recurrent patterns is that strong MCV almost always occurs at glacial inception and continues through the period of ice growth under conditions of declining insolation forced mainly by obliquity and secondarily by precession and CO₂. During the MPT (1.2-0.65 Ma), obliquity continues to influence MCV but in a non-linear fashion evidenced by the appearance of combination tones (28 kyrs) of the 41-kyr cycle (Figs. 9 and 10) in the power spectrum of MCV amplitude modulation. Near the end of the MPT at 650 ka, MCV amplitude modulation by obliquity wanes as quasi-periodic 100 kyr and precession power increases. Precession plays a greater role in modulating the amplitude of MCV in the late Pleistocene consistent with the steady increase in precession power throughout the Quaternary (Liautaud et al., 2020).



1063
 1064 Dansgaard-Oeschger events during MIS 3 are the archetypal example of millennial variability
 1065 and considerable effort has been directed towards documenting these events globally, including
 1066 the use of numerical models to understand their cause(s). MIS 3 is exceptional relative to the
 1067 other latest Pleistocene glaciations in terms of the high number of millennial events and there
 1068 appears to be no period like it during the past 1200 ka. The strong, continuous millennial
 1069 variability exhibited during MIS 3 is more similar to the millennial variability observed during
 1070 glacial cycles of the early Pleistocene from 1440 to 1200 ka (Birner et al., 2016). This similarity
 1071 is not entirely unexpected considering that benthic $\delta^{18}\text{O}$ values were about the same during
 1072 early Pleistocene glacial stages as those during MIS 3, indicating the climate system spent a
 1073 prolonged time in an intermediate glacial state. Our analysis of MCV at Site U1385 supports
 1074 the concept of a millennial window or sweet spot defined by a lower benthic $\delta^{18}\text{O}$ threshold of
 1075 $\sim 2.9\text{‰}$ below which MCV is suppressed during full interglacial conditions. The upper benthic
 1076 $\delta^{18}\text{O}$ threshold is less robust despite the fact that some glacial cycles in the late Pleistocene
 1077 show a clear pattern of reduced amplitude of MCV as the glacial maximum is approached.
 1078 Although the exact physical significance of the benthic $\delta^{18}\text{O}$ threshold remains uncertain with
 1079 many candidates (ice volume, ice height, sea level, sea ice, deep-water temperatures, etc.),
 1080 MCV is strongest during intermediate glacial states.

1081
 1082 Climate variability on orbital and suborbital time scales are coupled and interact in both
 1083 directions. An example of downscale interaction is the modulation of the amplitude and/or
 1084 frequency of MCV by Earth's orbital configuration either through the direct effects of
 1085 insolation or more indirectly through ice sheet growth. Some MCV may also be related to
 1086 harmonics or combination tones of the orbital cycle (Hagelberg et al., 1994). MCV can exert
 1087 an upscale influence on orbital times scales through its effect on ice sheet dynamics (Verbitsky
 1088 et al., 2019) or on atmospheric CO_2 by changing carbon storage in the deep-sea. MCV is also
 1089 a source of noise on glacial-interglacial timescales that may affect the resonance of internal
 1090 climate change with external orbital forcing.

1091
 1092 In addition to documenting MCV, the planktic and benthic isotope records from Site U1385
 1093 provide unprecedented detail of the amplitude and shapes (waveforms) of the glacial cycles on
 1094 orbital time scales for the last 1.45 Ma. We emphasize our record is from a single site and
 1095 should be compared with other records from higher latitude in the North Atlantic (e.g., Barker
 1096 et al., 2021, 2022) and elsewhere (Sun et al., 2021) in order to map geographical differences



1097 over time and develop confidence in the palaeoceanographic interpretations set out here. This
1098 study is also limited to the last 1.45 Ma and we cannot determine the extent to which MCV
1099 was present during glacial periods beyond this time. One of the objectives of upcoming IODP
1100 Expedition 397 is to return to the Iberian margin and extend the U1385 record to study how
1101 orbital and millennial variability co-evolved during through the Quaternary and Pliocene
1102 (Hodell et al., 2022). Understanding these interactions of climate on orbital and suborbital time
1103 scales will lead to a fuller understanding of the mechanisms responsible for the Quaternary ice
1104 ages.

1105

1106 **Data availability**

1107 All datasets and age models have been deposited with PANGAEA as 'in review' and will be
1108 publically available when the paper is accepted and a DOI is issued.

1109

1110 **Author contributions**

1111 DAH led the effort to drill Site U1385 and LL and DAH were shipboard scientists aboard IODP
1112 Expedition 393 that recovered the cores. LL constructed the spliced composite section for Site
1113 U1385. MJV provided taxonomic expertise and MJV and NT selected foraminifera and
1114 prepared samples for stable isotope analysis. JER and JN operated the mass spectrometers and
1115 produced the stable isotope data. LL, SJC and DAH oversaw the XRF analyses of the cores.
1116 LCS, PCT and VM provided data and interpretation of Core MD01-2444. EWW advised on
1117 the correlation of the marine sediment record to the Greenland and Antarctic ice cores. DAH,
1118 PCT and EWW wrote the first draft and all authors contributed to the submitted manuscript.

1119

1120 **Competing interests**

1121
1122 Two of the (co-)authors are a member of the editorial board of *Climate of the Past*. The peer-
1123 review process was guided by an independent editor, and the authors also have no other
1124 competing interests to declare.

1125

1126 **Disclaimer**

1127 Publisher's note: Copernicus Publications remains neutral with regard to jurisdictional claims
1128 in published maps and institutional affiliations.

1129

1130

1131

1132



Acknowledgments

Samples were provided by the International Ocean Discovery Program (IODP). We thank the IODP Expedition 393 drilling crew, ship's crew, and scientific and technical staff of the drillship *JOIDES Resolution* without whom recovering Site U1385 would not have been possible. We thank Jeannie Booth and Ian Mather for laboratory support. This research was supported by the Natural Environmental Research Council Grants NE/J00653X/1, NE/K005804/1, NE/J017922/1 and NE/R000204/1 and Leverhulme Trust Project RPG2014-417.

References:

- Ahn, J. and Brook, E. J.: Siple Dome ice reveals two modes of millennial CO₂ change during the last ice age, *Nature Communications*, 5, 3723, doi:10.1038/ncomms4723, URL <https://doi.org/10.1038/ncomms4723>, 2014.
- Alley, R. B.: Wally was right: Predictive ability of the North Atlantic “Conveyor Belt” hypothesis for abrupt climate change, *Annual Review of Earth and Planetary Sciences*, 35, 241–272, doi:10.1146/annurev.earth.35.081006.131524, URL <https://doi.org/10.1146/annurev.earth.35.081006.131524>, 2007.
- Alonso-Garcia, M., Sierro, F., Kucera, M., Flores, J., Cacho, I., and Andersen, N.: Ocean circulation, ice sheet growth and inter- hemispheric coupling of millennial climate variability during the mid-Pleistocene (ca 800–400ka), *Quaternary Science Reviews*, 30, 3234–3247, doi:<https://doi.org/10.1016/j.quascirev.2011.08.005>, URL <https://www.sciencedirect.com/science/article/pii/S0277379111002435>, 2011.
- Anderson, R. F., Ali, S., Bradtmiller, L. I., Nielsen, S. H. H., Fleisher, M. Q., Anderson, B. E., and Burckle, H.: Wind-driven upwelling in the Southern Ocean and the deglacial rise in atmospheric CO₂, *Science*, 323, 1443–1448, doi:10.1126/science.1167441, URL <https://www.science.org/doi/abs/10.1126/science.1167441>, 2009.
- Bajo, P., Drysdale, R. N., Woodhead, J. D., Hellstrom, J. C., Hodell, D.A., Ferretti, P., Voelker, A. H. L., Zanchetta, G., Rodrigues, T., Wolff, E. W., Tyler, J., Frisia, S., Spotl, C., and Fallick, A. E.: Persistent influence of obliquity on ice age terminations since the Middle Pleistocene transition, *Science*, 367, 1235–1239, doi:10.1126/science.aaw1114, URL <https://www.science.org/doi/abs/10.1126/science.aaw1114>, 2020.
- Barker, S., Starr, A., van der Lubbe, J., Doughty, A., Knorr, G., Conn, S., Lordsmith, S., Owen, L., Nederbragt, A., Hemming, S., Hall, I., Levay, L., null null, Berke, M. A., Brentegani, L., Caley, T., Cartagena-Sierra, A., Charles, C. D., Coenen, J. J., Crespin, J. G., Franzese, A. M., Gruetzner, J., Han, X., Hines, S. K. V., Espejo, F. J. J., Just, J., Koutsodendris, A., Kubota, K., Lathika, N., Norris, R. D., dos Santos, T. P., Robinson, R., Rolison, J. M., Simon, M. H., Tangunan, D., Yamane, M., and Zhang, H.: Persistent influence of precession on northern ice sheet variability since the early



- 1178 Pleistocene, *Science*, 376, 961–967, doi:10.1126/science.abm4033, URL
 1179 <https://www.science.org/doi/abs/10.1126/science.abm4033>, 2022.
 1180
 1181 Barker, S. and Knorr, G.: Millennial scale feedbacks determine the shape and rapidity of
 1182 glacial termination, *Nature Communications*, 12, 2273, doi:10.1038/s41467-021-
 1183 22388-6, 2021.
 1184
 1185 Barker, Knorr, Edwards, Parrenin, Putnam, Skinner, Wolff, and Ziegler] Barker, S., Knorr,
 1186 G., Edwards, R., Parrenin, F., Putnam, A., Skinner, L., Wolff, E., and Ziegler, M.:
 1187 800,000 years of abrupt climate variability, *Science*, 334, 347–51,
 1188 doi:10.1126/science.1203580, 2011.
 1189
 1190 Barker, S., Chen, J., Gong, X., Jonkers, L., Knorr, G., and Thornalley, D.: Icebergs not the
 1191 trigger for North Atlantic cold events, *Nature*, 520, 333–336,
 1192 doi:10.1038/nature14330, URL <https://doi.org/10.1038/nature14330>, 2015.
 1193
 1194 Barker, S., Zhang, X., Jonkers, L., Lordsmith, S., Conn, S., and Knorr, G.: Strengthening
 1195 Atlantic inflow across the mid- Pleistocene Transition, *Paleoceanography and*
 1196 *Paleoclimatology*, 36, e2020PA004 200, doi:<https://doi.org/10.1029/2020PA004200>,
 1197 URL <https://agupubs.onlinelibrary.wiley.com/doi/abs/10.1029/2020PA004200>,
 1198 e2020PA004200 2020PA004200, 2021.
 1199
 1200 Batchelor, C. L., Margold, M., Krapp, M., Murton, D. K., Dalton, A. S., Gibbard, P. L.,
 1201 Stokes, C. R., Murton, J. B., and Manica, A.: The configuration of Northern
 1202 Hemisphere ice sheets through the Quaternary, *Nature Communications*, 10, 3713,
 1203 doi:10.1038/s41467-019-11601-2, URL <https://doi.org/10.1038/s41467-019-11601-2>,
 1204 2019.
 1205
 1206 Bauska, T. K., Marcott, S. A., and Brook, E. J.: Abrupt changes in the global carbon cycle
 1207 during the last glacial period, *Nature Geoscience*, 14, 91–96, doi:10.1038/s41561-
 1208 020-00680-2, URL <https://doi.org/10.1038/s41561-020-00680-2>, 2021.
 1209
 1210 Bender, M., Sowers, T., Dickson, M.-L., Orchardo, J., Grootes, P., Mayewski, P. A., and
 1211 Meese, D. A.: Climate correlations between Greenland and Antarctica during the past
 1212 100,000 years, *Nature*, 372, 663–666, doi:10.1038/372663a0, URL
 1213 <https://doi.org/10.1038/372663a0>, 1994.
 1214
 1215 Benzi, R., Parisi, G., Sutera, A., and Vulpiani, A.: Stochastic resonance in climatic change,
 1216 *Tellus*, 34, 10–16, doi:<https://doi.org/10.1111/j.2153-3490.1982.tb01787.x>, 1982.
 1217
 1218 Berger, A., Loutre, M. F., and Melice, J. L.: Equatorial insolation: from precession harmonics
 1219 to eccentricity frequencies, *Climate of the Past*, 2, 131–136, doi:10.5194/cp-2-131-
 1220 2006, URL <https://cp.copernicus.org/articles/2/131/2006/>, 2006.
 1221
 1222 Billups, K. and Scheinwald, A.: Origin of millennial-scale climate signals in the subtropical
 1223 North Atlantic, *Paleoceanography*, 29, doi:10.1002/2014PA002641, 2014.
 1224
 1225 Birner, B., Hodell, D. A., Tzedakis, P. C., and Skinner, L. C.: Similar millennial climate
 1226 variability on the Iberian margin during two early Pleistocene glacials and MIS 3,



- 1227 Paleoclimatology, 31, 203–217, doi:<https://doi.org/10.1002/2015PA002868>, URL
 1228 <https://agupubs.onlinelibrary.wiley.com/doi/abs/10.1002/2015PA002868>, 2016.
 1229
- 1230 Blunier, T. and Brook, E. J.: Timing of millennial-scale climate change in Antarctica and
 1231 Greenland during the Last Glacial Period, *Science*, 291, 109–112,
 1232 doi:[10.1126/science.291.5501.109](https://doi.org/10.1126/science.291.5501.109), URL
 1233 <https://www.science.org/doi/abs/10.1126/science.291.5501.109>, 2001.
 1234
- 1235 Bolton, C. T., Bailey, I., Friedrich, O., Tachikawa, K., de Garidel-Thoron, T., Vidal, L.,
 1236 Sonzogni, C., Marino, G., Rohling, E. J., Robinson, M. M., Ermini, M., Koch, M.,
 1237 Cooper, M. J., and Wilson, P. A.: North Atlantic midlatitude surface-circulation
 1238 changes through the Plio-Pleistocene intensification of Northern Hemisphere
 1239 Glaciation, *Paleoclimatology and Paleoclimatology*, 33, 1186–1205,
 1240 doi:<https://doi.org/10.1029/2018PA003412>, URL
 1241 <https://agupubs.onlinelibrary.wiley.com/doi/abs/10.1029/2018PA003412>, 2018.
 1242
- 1243 Bond, G., Heinrich, H., Broecker, W., Labeyrie, L., McManus, J., Andrews, J., Huon, S.,
 1244 Jantschik, R., Clasen, S., Simet, C., Tedesco, K., Klas, M., Bonani, G., and Ivy,
 1245 S.: Evidence for massive discharges of icebergs into the North Atlantic ocean during
 1246 the last glacial period, *Nature*, 360, 245–249, doi:[10.1038/360245a0](https://doi.org/10.1038/360245a0), URL
 1247 <https://doi.org/10.1038/360245a0>, 1992.
 1248
- 1249 Bond, G., Broecker, W., Johnsen, S., McManus, J., Labeyrie, L., Jouzel, J., and Bonani, G.:
 1250 Correlations between climate records from North Atlantic sediments and Greenland
 1251 ice, *Nature*, 365, 143–147, doi:[10.1038/365143a0](https://doi.org/10.1038/365143a0), URL
 1252 <https://doi.org/10.1038/365143a0>, 1993.
 1253
- 1254 Broecker, W., Bond, G., Klas, M., Clark, E., and McManus, J.: Origin of the northern
 1255 Atlantic's Heinrich events, *Climate Dynamics*, 6, 265–273, doi:[10.1007/BF00193540](https://doi.org/10.1007/BF00193540),
 1256 URL <https://doi.org/10.1007/BF00193540>, 1992.
 1257
- 1258 Broecker, W. S. and van Donk, J.: Insolation changes, ice volumes, and the O18 record in
 1259 deep-sea cores, *Reviews of Geophysics*, 8, 169–198,
 1260 doi:<https://doi.org/10.1029/RG008i001p00169>, URL
 1261 <https://agupubs.onlinelibrary.wiley.com/doi/abs/10.1029/RG008i001p00169>, 1970.
 1262
- 1263 Broecker, W. S., Bond, G., Klas, M., Bonani, G., and Wolfli, W.: A salt oscillator in the
 1264 glacial Atlantic? 1. The concept, *Paleoclimatology*, 5, 469–477,
 1265 doi:<https://doi.org/10.1029/PA005i004p00469>, URL
 1266 <https://agupubs.onlinelibrary.wiley.com/doi/abs/10.1029/PA005i004p00469>, 1990.
 1267
- 1268 Brown, N. and Galbraith, E. D.: Hosed vs. unhosed: interruptions of the Atlantic Meridional
 1269 Overturning Circulation in a global coupled model, with and without freshwater
 1270 forcing, *Climate of the Past*, 12, 1663–1679, doi:[10.5194/cp-12-1663-2016](https://doi.org/10.5194/cp-12-1663-2016), URL
 1271 <https://cp.copernicus.org/articles/12/1663/2016/>, 2016.
 1272
- 1273 Buizert, C. and Schmittner, A.: Southern Ocean control of glacial AMOC stability and
 1274 Dansgaard-Oeschger interstadial duration, *Paleoclimatology*, 30, 1595–1612,
 1275 doi:<https://doi.org/10.1002/2015PA002795>, URL
 1276 <https://agupubs.onlinelibrary.wiley.com/doi/abs/10.1002/2015PA002795>, 2015.



- 1277
 1278 Burns, S. J., Welsh, L. K., Scroxton, N., Cheng, H., and Edwards, R. L.: Millennial
 1279 and orbital scale variability of the South American Monsoon during the penultimate
 1280 glacial period, *Scientific Reports*, 9, 1234, doi:10.1038/s41598-018-37854-3, URL
 1281 <https://doi.org/10.1038/s41598-018-37854-3>, 2019.
 1282
 1283 Chalk, T. B., Hain, M. P., Foster, G. L., Rohling, E. J., Sexton, P. F., Badger, M. P. S.,
 1284 Cherry, S. G., Hasenfratz, A. P., Haug, G. H., Jaccard, S. L., Martinez-Garcia, A.,
 1285 Palike, H., Pancost, R. D., and Wilson, P. A.: Causes of ice age intensification across
 1286 the Mid-Pleistocene Transition, *Proceedings of the National Academy of Sciences*,
 1287 114, 13,114–13,119, doi:10.1073/pnas.1702143114, URL
 1288 <https://www.pnas.org/doi/abs/10.1073/pnas.1702143114>, 2017.
 1289
 1290 Channell, J., Hodell, D., Romero, O., Hillaire-Marcel, C., de Vernal, A., Stoner, J., Mazaud,
 1291 A., and Rohl, U.: A 750-kyr detrital-layer stratigraphy for the North Atlantic (IODP
 1292 Sites U1302–U1303, Orphan Knoll, Labrador Sea), *Earth and Planetary Science*
 1293 *Letters*, 317–318, 218–230, doi:<https://doi.org/10.1016/j.epsl.2011.11.029>, URL
 1294 <https://www.sciencedirect.com/science/article/pii/S0012821X11006868>, 2012.
 1295
 1296 Channell, J., Hodell, D., Crowhurst, S., Skinner, L., and Muscheler, R.: Relative
 1297 paleointensity (RPI) in the latest Pleistocene (10–45 ka) and implications for
 1298 deglacial atmospheric radiocarbon, *Quaternary Science Reviews*, 191, 57–72,
 1299 doi:<https://doi.org/10.1016/j.quascirev.2018.05.007>, URL
 1300 <https://www.sciencedirect.com/science/article/pii/S0277379118302828>, 2018.
 1301
 1302 Clark, P. U., Archer, D., Pollard, D., Blum, J. D., Rial, J. A., Brovkin, V., Mix, A. C., Pisias,
 1303 N. G., and Roy, M.: The middle Pleistocene transition: characteristics, mechanisms,
 1304 and implications for long-term changes in atmospheric pCO₂, *Quaternary Science*
 1305 *Reviews*, 25, 3150–3184, doi:<https://doi.org/10.1016/j.quascirev.2006.07.008>, URL
 1306 <https://www.sciencedirect.com/science/article/pii/S0277379106002332>, critical
 1307 *Quaternary Stratigraphy*, 2006.
 1308
 1309 Dansgaard, W., Clausen, H. B., Gundestrup, N., Hammer, C. U., Johnsen, S. F.,
 1310 Kristinsdottir, P. M., and Reeh, N.: A new Greenland deep ice core, *Science*, 218,
 1311 1273–1277, doi:10.1126/science.218.4579.1273, URL
 1312 <https://www.science.org/doi/abs/10.1126/science.218.4579.1273>, 1982.
 1313
 1314 DeBoer, A. M. and Nof, D.: The Bering Strait’s grip on the northern hemisphere climate,
 1315 *Deep Sea Research Part I: Oceanographic Research Papers*, 51, 1347–1366,
 1316 doi:<https://doi.org/10.1016/j.dsr.2004.05.003>, URL
 1317 <https://www.sciencedirect.com/science/article/pii/S0967063704000901>, 2004.
 1318
 1319 de Verdiere, A.C.: A simple model of millennial oscillations of the thermohaline circulation,
 1320 *Journal of Physical Oceanography*, 37, 1142–1155, doi:10.1175/JPO3056.1, URL
 1321 <https://journals.ametsoc.org/view/journals/phoc/37/5/jpo3056.1.xml>, 2007.
 1322
 1323 Dokken, T. M., Nisancioglu, K. H., Li, C., Battisti, D. S., and Kissel, C.: Dansgaard-
 1324 Oeschger cycles: Interactions between ocean and sea ice intrinsic to the Nordic seas,
 1325 *Paleoceanography*, 28, 491–502, doi:<https://doi.org/10.1002/palo.20042>, URL
 1326 <https://agupubs.onlinelibrary.wiley.com/doi/abs/10.1002/palo.20042>, 2013.



- 1327
 1328 Duplessy, J.-C., Labeyrie, L., and Waelbroeck, C.: Constraints on the ocean
 1329 oxygen isotopic enrichment between the Last Glacial Maximum and the
 1330 Holocene: Paleoceanographic implications, *Quaternary Science Reviews*,
 1331 21, 315–330, doi:[https://doi.org/10.1016/S0277-3791\(01\)00107-X](https://doi.org/10.1016/S0277-3791(01)00107-X), URL
 1332 <https://www.sciencedirect.com/science/article/pii/S027737910100107X>,
 1333 ePILOG, 2002.
 1334
 1335 Dyez, K. A., Honisch, B., and Schmidt, G. A.: Early Pleistocene obliquity-scale pCO₂
 1336 variability at 1.5 million years ago, *Paleoceanography and Paleoclimatology*, 33,
 1337 1270–1291, doi:<https://doi.org/10.1029/2018PA003349>, URL
 1338 <https://agupubs.onlinelibrary.wiley.com/doi/abs/10.1029/2018PA003349>, 2018.
 1339
 1340 Elderfield, H., Ferretti, P., Greaves, M., Crowhurst, S., McCave, I. N., Hodell, D., and
 1341 Piotrowski, A. M.: Evolution of ocean temperature and ice volume through the Mid-
 1342 Pleistocene Climate Transition, *Science*, 337, 704–709, doi:10.1126/science.1221294,
 1343 URL <https://www.science.org/doi/abs/10.1126/science.1221294>, 2012.
 1344
 1345 EPICA Community Members: Eight glacial cycles from an Antarctic ice core, *Nature*, 429,
 1346 623–628, doi:10.1038/nature02599, URL <https://doi.org/10.1038/nature02599>, 2004.
 1347
 1348 Ferretti, P., Crowhurst, S. J., Naafs, B. D. A., and Barbante, C.: The Marine Isotope Stage 19
 1349 in the mid-latitude North Atlantic Ocean: astronomical signature and intra-interglacial
 1350 variability, *Quaternary Science Reviews*, 108, 95–110,
 1351 doi:<https://doi.org/10.1016/j.quascirev.2014.10.024>, URL
 1352 <https://www.sciencedirect.com/science/article/pii/S0277379114004119>, 2015.
 1353
 1354 Friedrich, T., Timmermann, A., Menviel, L., Elison Timm, O., Mouchet, A., and Roche,
 1355 D. M.: The mechanism behind internally generated centennial-to-millennial scale
 1356 climate variability in an earth system model of intermediate complexity,
 1357 *Geoscientific Model Development*, 3, 377–389, doi:10.5194/gmd-3-377-2010,
 1358 URL <https://gmd.copernicus.org/articles/3/377/2010/>, 2010.
 1359
 1360 Galaasen, E., Ninnemann, U., Kessler, A., Irvali, N., Rosenthal, Y., Tjiputra, J., Bouttes, N.,
 1361 Roche, D., Kleiven, K. H., and Hodell, D.: Interglacial instability of North Atlantic
 1362 Deep Water ventilation, *Science*, 367, 1485–1489, doi:10.1126/science.aay6381,
 1363 2020.
 1364
 1365 Galaasen, E. V., Ninnemann, U. S., Irvali, N., Kleiven, H. K. F., Rosenthal, Y., Kissel, C.,
 1366 and Hodell, D. A.: Rapid reductions in North Atlantic Deep Water during the peak of
 1367 the last interglacial period, *Science*, 343, 1129–1132, doi:10.1126/science.1248667,
 1368 URL <https://www.science.org/doi/abs/10.1126/science.1248667>, 2014.
 1369
 1370 Galbraith, E. D. and de Lavergne, C.: Response of a comprehensive climate model to a broad
 1371 range of external forcings: relevance for deep ocean ventilation and the development
 1372 of late Cenozoic ice ages, *Climate Dynamics*, 52, 653–679, 2018.
 1373
 1374 Ganopolski, A. and Rahmstorf, S.: Rapid changes of glacial climate simulated in a
 1375 coupled climate model, *Nature*, 409, 153–158, doi:10.1038/35051500, URL
 1376 <https://doi.org/10.1038/35051500>, 2001.



- 1377
 1378 Gebbie, G.: Tracer transport timescales and the observed Atlantic-Pacific lag in the timing of
 1379 the Last Termination, *Paleoceanography*, 27,
 1380 doi:<https://doi.org/10.1029/2011PA002273>, URL
 1381 <https://agupubs.onlinelibrary.wiley.com/doi/abs/10.1029/2011PA002273>,
 1382 2012.
 1383
 1384 Gildor, H. and Tziperman, E.: A sea ice climate switch mechanism for the 100-kyr glacial
 1385 cycles, *Journal of Geophysical Research*, 106, doi:10.1029/1999JC000120, 2001.
 1386
 1387 Gottschalk, Skinner, Jaccard, Menviel, Nehrbass-Ahles, and Waelbroeck]
 1388 Gottschalk, J., Skinner, L. C., Jaccard, S. L., Menviel, L., Nehrbass-
 1389 Ahles, C., and Waelbroeck, C.: Southern Ocean link between changes
 1390 in atmospheric CO₂ levels and northern-hemisphere climate anomalies
 1391 during the last two glacial periods, *Quaternary Science Reviews*, 230, 106 067,
 1392 doi:<https://doi.org/10.1016/j.quascirev.2019.106067>, URL
 1393 <https://www.sciencedirect.com/science/article/pii/S0277379118310461>, 2020
 1394
 1395 Grutzner, J. and Higgins, S. M.: Threshold behavior of millennial scale variability in deep
 1396 water hydrography inferred from a 1.1 Ma long record of sediment provenance at the
 1397 southern Gardar Drift, *Paleoceanography*, 25,
 1398 doi:<https://doi.org/10.1029/2009PA001873>, URL
 1399 <https://agupubs.onlinelibrary.wiley.com/doi/abs/10.1029/2009PA001873>, 2010.
 1400
 1401 Haeberli, M., Baggenstos, D., Schmitt, J., Grimmer, M., Michel, A., Kellerhals, T., and
 1402 Fischer, H.: Snapshots of mean ocean temperature over the last 700 000 years using
 1403 noble gases in the EPICA Dome C ice core, *Climate of the Past*, 17, 843–867,
 1404 doi:10.5194/cp-17-843-2021, URL <https://cp.copernicus.org/articles/17/843/2021/>,
 1405 2021.
 1406
 1407 Hagelberg, T. K., Bond, G., and deMenocal, P.: Milankovitch band forcing of sub-
 1408 Milankovitch climate variability during the Pleistocene, *Paleoceanography*, 9, 545–
 1409 558, doi:<https://doi.org/10.1029/94PA00443>, URL
 1410 <https://agupubs.onlinelibrary.wiley.com/doi/abs/10.1029/94PA00443>, 1994.
 1411
 1412 Heinrich, H.: Origin and consequences of cyclic ice rafting in the Northeast Atlantic Ocean
 1413 during the past 130,000 years, *Quaternary Research*, 29, 142–152,
 1414 doi:[https://doi.org/10.1016/0033-5894\(88\)90057-9](https://doi.org/10.1016/0033-5894(88)90057-9), URL
 1415 <https://www.sciencedirect.com/science/article/pii/0033589488900579>, 1988.
 1416
 1417 Hemming, S. R.: Heinrich events: Massive late Pleistocene detritus layers of the North
 1418 Atlantic and their global climate imprint, *Reviews of Geophysics*, 42,
 1419 doi:<https://doi.org/10.1029/2003RG000128>, URL
 1420 <https://agupubs.onlinelibrary.wiley.com/doi/abs/10.1029/2003RG000128>, 2004.
 1421
 1422 Henry, L. G., McManus, J. F., Curry, W. B., Roberts, N. L., Piotrowski, A. M., and
 1423 Keigwin, L. D.: North Atlantic ocean circulation and abrupt climate change during
 1424 the last glaciation, *Science*, 353, 470–474, doi:10.1126/science.aaf5529, URL
 1425 <https://www.science.org/doi/abs/10.1126/science.aaf5529>, 2016.
 1426



- Higgins, J. A., Kurbatov, A. V., Spaulding, N. E., Brook, E., Introne, D. S., Chimiak, L. M., Yan, Y., Mayewski, P. A., and Bender, M. L.: Atmospheric composition 1 million years ago from blue ice in the Allan Hills, Antarctica, *Proceedings of the National Academy of Sciences*, 112, 6887–6891, doi:10.1073/pnas.1420232112, URL <https://www.pnas.org/doi/abs/10.1073/pnas.1420232112>, 2015.
- Hilborn, R. C. and Sprott, J. C.: Chaos and Nonlinear Dynamics: An Introduction for Scientists and Engineers, *American Journal of Physics*, 62, 861–862, doi:10.1119/1.17477, URL <https://doi.org/10.1119/1.17477>, 1994.
- Hinnov, L.A., Schulz, M., and Yiou, P.: Interhemispheric space–time attributes of the Dansgaard–Oeschger oscillations between 100 and 0 ka, *Quaternary Science Reviews*, 21, 1213–1228, 2002.
- Hinnov, L. A., Schulz, M., and Yiou, P.: Interhemispheric space–time attributes of the Dansgaard–Oeschger oscillations between 100 and 0 ka, *Quaternary Science Reviews*, 21, 1213–1228, doi:[https://doi.org/10.1016/S0277-3791\(01\)00140-8](https://doi.org/10.1016/S0277-3791(01)00140-8), URL <https://www.sciencedirect.com/science/article/pii/S0277379101001408>, 2002.
- Hodell, D.A., Abrantes, F., and Alvarez Zarikian, C.A.: *Expedition 397 Scientific Prospectus: Iberian Margin Paleoclimate*. International Ocean Discovery Program. <https://doi.org/10.14379/iodp.sp.397.2022>, 2022.
- Hodell, D., Crowhurst, S., Skinner, L., Tzedakis, P. C., Margari, V., Channell, J. E., Kamenov, G., Maclachlan, S., and Rothwell, G.: Response of Iberian Margin sediments to orbital and suborbital forcing over the past 420ka, *Paleoceanography*, 28, 185–199, doi:<https://doi.org/10.1002/palo.20017>, URL <https://agupubs.onlinelibrary.wiley.com/doi/abs/10.1002/palo.20017>, 2013.
- Hodell, D., Lourens, L., Crowhurst, S., Konijnendijk, T., Tjallingii, R., Jimenez-Espejo, F., Skinner, L., Tzedakis, P., Abrantes, F., Acton, G. D., Alvarez Zarikian, C. A., Bahr, A., Balestra, B., Barranco, E. L., Carrara, G., Ducassou, E., Flood, R. D., Flores, J.-A., Furota, S., Grimalt, J., Grunert, P., Hernandez-Molina, J., Kim, J. K., Krissek, L. A., Kuroda, J., Li, B., Lofi, J., Margari, V., Martrat, B., Miller, M. D., Nanayama, F., Nishida, N., Richter, C., Rodrigues, T., Rodriguez-Tovar, F. J., Roque, A. C. F., Sanchez Goni, M. F., Sierro Sanchez, F. J., Singh, A. D., Sloss, C. R., Stow, D. A., Takashimizu, Y., Tzanova, A., Voelker, A., Xuan, C., and Williams, T.: A reference time scale for Site U1385 (Shackleton Site) on the SW Iberian Margin, *Global and Planetary Change*, 133, 49–64, doi:<https://doi.org/10.1016/j.gloplacha.2015.07.002>, URL <https://www.sciencedirect.com/science/article/pii/S0921818115001423>, 2015.
- Hodell, D. A. and Channell, J. E. T.: Mode transitions in Northern Hemisphere glaciation: co-evolution of millennial and orbital variability in Quaternary climate, *Climate of the Past*, 12, 1805–1828, doi:10.5194/cp-12-1805-2016, URL <https://cp.copernicus.org/articles/12/1805/2016/>, 2016.
- Hodell, D. A., Channell, J. E. T., Curtis, J. H., Romero, O. E., and Rohl, U.: Onset of “Hudson Strait” Heinrich events in the eastern North Atlantic at the end of the middle



- 1477 Pleistocene transition (640 ka)?, *Paleoceanography*, 23,
 1478 doi:<https://doi.org/10.1029/2008PA001591>, URL
 1479 <https://agupubs.onlinelibrary.wiley.com/doi/abs/10.1029/2008PA001591>, 2008.
 1480
- 1481 Hodell, D. A., Minth, E. K., Curtis, J. H., McCave, I. N., Hall, I. R., Channell, J. E., and
 1482 Xuan, C.: Surface and deep-water hydrography on Gardar Drift (Iceland Basin)
 1483 during the last interglacial period, *Earth and Planetary Science Letters*, 288, 10–19,
 1484 doi:<https://doi.org/10.1016/j.epsl.2009.08.040>, URL
 1485 <https://www.sciencedirect.com/science/article/pii/S0012821X09005147>, 2009.
 1486
- 1487 Honisch, B., Ridgwell, A., Schmidt, D. N., Thomas, E., Gibbs, S. J., Sluijs, A., Zeebe, R.,
 1488 Kump, L., Martindale, R. C., Greene, S. E., Kiessling, W., Ries, J., Zachos, J. C.,
 1489 Royer, D. L., Barker, S., Marchitto, T. M., Moyer, R., Pelejero, C., Ziveri, P.,
 1490 Foster, G. L., and Williams, B.: The geological record of ocean acidification, *Science*,
 1491 335, 1058–1063, doi:10.1126/science.1208277, URL
 1492 <https://www.science.org/doi/abs/10.1126/science.1208277>, 2012.
 1493
- 1494 Hoogakker, B., Elderfield, H., Oliver, K., and Crowhurst, S.: Benthic
 1495 foraminiferal oxygen isotope offsets over the last glacial-interglacial cycle,
 1496 *Paleoceanography*, 25, doi:<https://doi.org/10.1029/2009PA001870>, URL
 1497 <https://agupubs.onlinelibrary.wiley.com/doi/abs/10.1029/2009PA001870>, 2010.
 1498
- 1499 Hu, A., Meehl, G. A., Han, W., Abe-Ouchi, A., Morrill, C., Okazaki, Y., and Chikamoto,
 1500 M. O.: The Pacific-Atlantic seesaw and the Bering Strait, *Geophysical Research*
 1501 *Letters*, 39, doi:<https://doi.org/10.1029/2011GL050567>, URL
 1502 <https://agupubs.onlinelibrary.wiley.com/doi/abs/10.1029/2011GL050567>, 2012a.
 1503
- 1504 Hu, A., Meehl, G. A., Han, W., Timmermann, A., Otto-Bliesner, B., Liu, Z., Washington, W.
 1505 M., Large, W., Abe-Ouchi, A., Kimoto, M., Lambeck, K., and Wu, B.: Role of
 1506 the Bering Strait on the hysteresis of the ocean conveyor belt circulation and glacial
 1507 climate stability, *Proceedings of the National Academy of Sciences*, 109, 6417–6422,
 1508 doi:10.1073/pnas.1116014109, URL
 1509 <https://www.pnas.org/doi/abs/10.1073/pnas.1116014109>, 2012b.
 1510
- 1511 Huybers, P. and Curry, W.: Links between annual, Milankovitch and continuum
 1512 temperature variability, *Nature*, 441, 329–332, doi:10.1038/nature04745, URL
 1513 <https://doi.org/10.1038/nature04745>, 2006.
 1514
- 1515 Huybers, P. and Wunsch, C.: A depth-derived Pleistocene age model: Uncertainty estimates,
 1516 sedimentation variability, and nonlinear climate change, *Paleoceanography*, 19,
 1517 doi:<https://doi.org/10.1029/2002PA000857>, URL
 1518 <https://agupubs.onlinelibrary.wiley.com/doi/abs/10.1029/2002PA000857>,
 1519 2004.
 1520
- 1521 Jansen, M. F., Nadeau, L.-P., and Merlis, T. M.: Transient versus equilibrium response of the
 1522 ocean’s overturning circulation to warming, *Journal of Climate*, 31, 5147 – 5163,
 1523 doi:10.1175/JCLI-D-17-0797.1, URL
 1524 <https://journals.ametsoc.org/view/journals/clim/31/13/jcli-d-17-0797.1.xml>, 2018.
 1525



- Jouzel, J., Masson-Delmotte, V., Cattani, O., Dreyfus, G., Falourd, S., Hoffmann, G.,
 Minster, B., Nouet, J., Barnola, J. M., Chappellaz, J., Fischer, H., Gallet, J. C.,
 Johnsen, S., Leuenberger, M., Loulergue, L., Luethi, D., Oerter, H., Parrenin, F.,
 Raisbeck, G., Raynaud, D., Schilt, A., Schwander, J., Selmo, E., Souchez, R.,
 Spahni, R., Stauffer, B., Steffensen, J. P., Stenni, B., Stocker, T. F., Tison, J. L.,
 Werner, M., and Wolff, E. W.: Orbital and millennial Antarctic climate variability
 over the past 800,000 years, *Science*, 317, 793–796, doi:10.1126/science.1141038,
 URL <https://www.science.org/doi/abs/10.1126/science.1141038>, 2007.
- Kawamura, K., Abe-Ouchi, A., Motoyama, H., Ageta, Y., Aoki, S., Azuma, N., Fujii, Y.,
 Fujita, K., Fujita, S., Fukui, K., Furukawa, T., Furusaki, A., Goto-Azuma, K.,
 Greve, R., Hirabayashi, M., Hondoh, T., Hori, A., Horikawa, S., Horiuchi, K.,
 Igarashi, M., Iizuka, Y., Kameda, T., Kanda, H., Kohno, M., Kuramoto, T., Matsushi,
 Y., Miyahara, M., Miyake, T., Miyamoto, A., Nagashima, Y., Nakayama, Y.,
 Nakazawa, T., Nakazawa, F., Nishio, F., Obinata, I., Ohgaito, R., Oka, A., Okuno,
 J., Okuyama, J., Oyabu, I., Parrenin, F., Pattyn, F., Saito, F., Saito, T., Saito, T.,
 Sakurai, T., Sasa, K., Seddik, H., Shibata, Y., Shinbori, K., Suzuki, K., Suzuki, T.,
 Takahashi, A., Takahashi, K., Takahashi, S., Takata, M., Tanaka, Y., Uemura, R.,
 Watanabe, G., Watanabe, O., Yamasaki, T., Yokoyama, K., Yoshimori, M., and
 Yoshimoto, T.: State dependence of climatic instability over the past 720,000 years
 from Antarctic ice cores and climate modeling, *Science Advances*, 3, e1600 446,
 doi:10.1126/sciadv.1600446, URL
<https://www.science.org/doi/abs/10.1126/sciadv.1600446>, 2017.
- Kleppin, H., Jochum, M., Otto-Bliesner, B., Shields, C. A., and Yeager, S.: Stochastic
 atmospheric forcing as a cause of Greenland climate transitions, *Journal of Climate*,
 28, 7741–7763, doi:10.1175/JCLI-D-14-00728.1, URL
<https://journals.ametsoc.org/view/journals/clim/28/19/jcli-d-14-00728.1.xml>, 2015.
- Larrasoana, J., Roberts, A., Rohling, E., Winkhofer, M., and Wehausen, R.: Three million
 years of monsoon variability over the northern Sahara, *Climate Dynamics*, 21, 689–
 698, doi:10.1007/s00382-003-0355-z, 2003.
- Li, C., Battisti, D. S., Schrag, D. P., and Tziperman, E.: Abrupt climate shifts in Greenland
 due to displacements of the sea ice edge, *Geophysical Research Letters*, 32,
 doi:<https://doi.org/10.1029/2005GL023492>, URL
<https://agupubs.onlinelibrary.wiley.com/doi/abs/10.1029/2005GL023492>, 2005.
- Li, C., Battisti, D. S., and Bitz, C. M.: Can North Atlantic sea ice anomalies account for
 Dansgaard–Oeschger climate signals?, *Journal of Climate*, 23, 5457–5475,
 doi:10.1175/2010JCLI3409.1, URL
<https://journals.ametsoc.org/view/journals/clim/23/20/2010jcli3409.1.xml>, 2010.
- Li, M., Hinnov, L., and Kump, L.: Acycle: Time-series analysis software for paleoclimate
 research and education, *Computers Geosciences*, 127, 12–22, doi:
 10.1016/j.cageo.2019.02.011, 2019.
- Liautaud, P. R., Hodell, D. A., and Huybers, P. J.: Detection of significant climatic
 precession variability in early Pleistocene glacial cycles, *Earth and Planetary*



- 1575 Science Letters, 536, 116–137, doi:<https://doi.org/10.1016/j.epsl.2020.116137>, URL
 1576 <https://www.sciencedirect.com/science/article/pii/S0012821X20300807>, 2020.
 1577
 1578 Liebrand, D. and de Bakker, A. T. M.: Bispectra of climate cycles show how ice ages are
 1579 fuelled, *Climate of the Past*, 15, 1959–1983, doi:10.5194/cp-15-1959-2019, URL
 1580 <https://cp.copernicus.org/articles/15/1959/2019/>, 2019.
 1581
 1582 Lisiecki, L. E. and Raymo, M. E.: A Pliocene-Pleistocene stack of 57 globally distributed
 1583 benthic $\delta^{18}\text{O}$ records, *Paleoceanography*, 20,
 1584 doi:<https://doi.org/10.1029/2004PA001071>, URL
 1585 <https://agupubs.onlinelibrary.wiley.com/doi/abs/10.1029/2004PA001071>,
 1586 2005.
 1587
 1588 Liu, J., Mao, J., Huang, B., and Liu, P.: Chaos and reverse transitions in stochastic
 1589 resonance, *Physics Letters A*, 382, 3071–3078,
 1590 doi:<https://doi.org/10.1016/j.physleta.2018.08.016>, URL
 1591 <https://www.sciencedirect.com/science/article/pii/S0375960118308880>, 2018.
 1592
 1593 Louergue, L., Schilt, A., Spahni, R., Masson-Delmotte, V., Blunier, T., Lemieux, B.,
 1594 Barnola, J.-M., Raynaud, D., Stocker, T. F., and Chappellaz, J.: Orbital and
 1595 millennial-scale features of atmospheric CH_4 over the past 800,000 years, *Nature*,
 1596 453, 383–386, doi:10.1038/nature06950, URL <https://doi.org/10.1038/nature06950>,
 1597 2008.
 1598
 1599 Lourens, L. J., Becker, J., Bintanja, R., Hilgen, F. J., Tüenter, E., van de Wal, R. S., and
 1600 Ziegler, M.: Linear and non-linear response of late Neogene glacial cycles to
 1601 obliquity forcing and implications for the Milankovitch theory, *Quaternary Science*
 1602 *Reviews*, 29, 352–365, doi:<https://doi.org/10.1016/j.quascirev.2009.10.018>, URL
 1603 <https://www.sciencedirect.com/science/article/pii/S0277379109003631>, 2010.
 1604
 1605 Luthi, D., Le Floch, M., Bereiter, B., Blunier, T., Barnola, J.-M., Siegenthaler, U., Raynaud,
 1606 D., Jouzel, J., Fischer, H., Kawamura, K., and Stocker, T. F.: High-resolution carbon
 1607 dioxide concentration record 650,000–800,000 years before present, *Nature*, 453,
 1608 379–382, doi: 10.1038/nature06949, URL <https://doi.org/10.1038/nature06949>, 2008.
 1609
 1610 Lynch-Stieglitz, J.: The Atlantic meridional overturning circulation and abrupt climate
 1611 change, *Annual Review of Marine Science*, 9, 83–104, doi:10.1146/annurev-marine-
 1612 010816-060415, URL <https://doi.org/10.1146/annurev-marine-010816-060415>,
 1613 PMID: 27814029, 2017.
 1614
 1615 Mangerud, J.: The discovery of the Younger Dryas, and comments on the current meaning
 1616 and usage of the term, *Boreas*, 50, 1–5, doi:<https://doi.org/10.1111/bor.12481>, URL
 1617 <https://onlinelibrary.wiley.com/doi/abs/10.1111/bor.12481>, 2021.
 1618
 1619 Mantsis, D. F., Clement, A. C., Broccoli, A. J., and Erb, M. P.: Climate feedbacks in
 1620 response to changes in obliquity, *Journal of Climate*, 24, 2830–2845,
 1621 doi:10.1175/2010JCLI3986.1, URL
 1622 <https://journals.ametsoc.org/view/journals/clim/24/11/2010jcli3986.1.xml>, 2011.
 1623



- Marcott, S. A., Bauska, T. K., Buizert, C., Steig, E. J., Rosen, J. L., Cuffey, K. M., Fudge, T. J., Severinghaus, J. P., Ahn, J., Kalk, M. L., McConnell, J. R., Sowers, T., Taylor, K. C., White, J. W. C., and Brook, E. J.: Centennial-scale changes in the global carbon cycle during the last deglaciation, *Nature*, 514, 616–619, doi:10.1038/nature13799, URL <https://doi.org/10.1038/nature13799>, 2014.
- Margari, V., Skinner, L. C., Tzedakis, P. C., Ganopolski, A., Vautravers, M., and Shackleton, N. J.: The nature of millennial-scale climate variability during the past two glacial periods, *Nature Geoscience*, 3, 127–131, doi:10.1038/ngeo740, URL <https://doi.org/10.1038/ngeo740>, 2010.
- Margari, V., Skinner, L., Hodell, D., Martrat, B., Toucanne, S., Gibbard, P., Lunkka, J., and Tzedakis, C.: Land-ocean changes on orbital and millennial time scales and the penultimate glaciation, *Geology*, doi:10.1130/G35070.1, 2014.
- Margari, V., Skinner, L. C., Menviel, L., Capron, E., Rhodes, R. H., Mleneck-Vautravers, M. J., Ezat, M. M., Martrat, B., Grimalt, J. O., Hodell, D. A., and Tzedakis, P. C.: Fast and slow components of interstadial warming in the North Atlantic during the last glacial, *Communications Earth & Environment*, 1, 6, doi:10.1038/s43247-020-0006-x, URL <https://doi.org/10.1038/s43247-020-0006-x>, 2020.
- Marshall, S. J. and Koutnik, M. R.: Ice Sheet Action Versus Reaction: Distinguishing between Heinrich Events and Dansgaard-Oeschger Cycles in the North Atlantic, *Paleoceanography*, 21, 1–13, 2006.
- Martinez-Boti, M. A., Foster, G. L., Chalk, T. B., Rohling, E. J., Sexton, P. F., Lunt, D. J., Pancost, R. D., Badger, M. P. S., and Schmidt, D. N.: Plio-Pleistocene climate sensitivity evaluated using high-resolution CO₂ records, *Nature*, 518, 49–54, doi:10.1038/nature14145, URL <https://doi.org/10.1038/nature14145>, 2015.
- Martrat, B., Grimalt, J. O., Shackleton, N. J., de Abreu, L., Hutterli, M. A., and Stocker, T. F.: Four climate cycles of recurring deep and surface water destabilizations on the Iberian Margin, *Science*, 317, 502–507, doi:10.1126/science.1139994, URL <https://www.science.org/doi/abs/10.1126/science.1139994>, 2007.
- McIntyre, K., Delaney, M. L., and Ravelo, A. C.: Millennial-scale climate change and oceanic processes in the Late Pliocene and Early Pleistocene, *Paleoceanography*, 16, 535–543, doi:<https://doi.org/10.1029/2000PA000526>, URL <https://agupubs.onlinelibrary.wiley.com/doi/abs/10.1029/2000PA000526>, 2001.
- McManus, J. F., Oppo, D. W., and Cullen, J. L.: A 0.5-million-year record of millennial-scale climate variability in the North Atlantic, *Science*, 283, 971–975, doi:10.1126/science.283.5404.971, URL <https://www.science.org/doi/abs/10.1126/science.283.5404.971>, 1999.
- McManus, J. F., Francois, R., Gherardi, J. M., Keigwin, L. D., and Brown-Leger, S.: Collapse and rapid resumption of Atlantic meridional circulation linked to deglacial climate changes, *Nature*, 428, 834–837, doi: 10.1038/nature02494, URL <https://doi.org/10.1038/nature02494>, 2004.



- 1674 Menviel, L. C., Skinner, L. C., Tarasov, L., and Tzedakis, P. C.: An ice–climate oscillatory
 1675 framework for Dansgaard–Oeschger cycles, *Nature Reviews Earth and Environment*,
 1676 1, 677–693, doi:10.1038/s43017-020-00106-y, URL [https://doi.org/10.1038/s43017-](https://doi.org/10.1038/s43017-020-00106-y)
 1677 020-00106-y, 2020.
- 1678
- 1679 Nehrbass-Ahles, C., Shin, J., Schmitt, J., Bereiter, B., Joos, F., Schilt, A., Schmidely, L.,
 1680 Silva, L., Teste, G., Grilli, R., Chappellaz, J., Hodell, D., Fischer, H., and Stocker,
 1681 T. F.: Abrupt CO₂ release to the atmosphere under glacial and early interglacial
 1682 climate conditions, *Science*, 369, 1000–1005, doi:10.1126/science.aay8178, URL
 1683 <https://www.science.org/doi/abs/10.1126/science.aay8178>, 2020.
- 1684
- 1685 Niu, L., Lohmann, G., and Gowan, E. J.: Climate noise influences ice sheet mean state,
 1686 *Geophysical Research Letters*, 46, 9690–9699,
 1687 doi:<https://doi.org/10.1029/2019GL083717>, URL
 1688 <https://agupubs.onlinelibrary.wiley.com/doi/abs/10.1029/2019GL083717>, 2019.
- 1689
- 1690 North Greenland Ice Core Project Members: High-resolution record of Northern Hemisphere
 1691 climate extending into the last interglacial period, *Nature*, 431, 147–151,
 1692 doi:10.1038/nature02805, URL <https://doi.org/10.1038/nature02805>, 2004.
- 1693
- 1694 Oliveira, D., Desprat, S., Rodrigues, T., Naughton, F., Hodell, D., Trigo, R., Rufino, M.,
 1695 Lopes, C., Abrantes, F., and Sanchez Goni, M.: The complexity of millennial-scale
 1696 variability in southwestern Europe during MIS 11, *Quaternary Research*, 86,
 1697 doi:10.1016/j.yqres.2016.09.002, 2016.
- 1698
- 1699 Oliveira, D., Sanchez Goni, M. F., Naughton, F., Polanco-Martinez, J., Jimenez-Espejo,
 1700 F. J., Grimalt, J. O., Martrat, B., Voelker, A. H., Trigo, R., Hodell, D., Abrantes, F.,
 1701 and Desprat, S.: Unexpected weak seasonal climate in the western Mediterranean
 1702 region during MIS 31, a high-insolation forced interglacial, *Quaternary Science*
 1703 *Reviews*, 161, 1–17, doi:<https://doi.org/10.1016/j.quascirev.2017.02.013>, URL
 1704 <https://www.sciencedirect.com/science/article/pii/S0277379116306515>, 2017.
- 1705
- 1706 Oppo, D. W., McManus, J. F., and Cullen, J. L.: Abrupt climate events 500,000 to 340,000
 1707 years ago: Evidence from subpolar North Atlantic sediments, *Science*, 279, 1335–
 1708 1338, doi:10.1126/science.279.5355.1335, URL
 1709 <https://www.science.org/doi/abs/10.1126/science.279.5355.1335>, 1998.
- 1710
- 1711 Pailler, D. and Bard, E.: High frequency palaeoceanographic changes during the past 140000
 1712 yr recorded by the organic matter in sediments of the Iberian Margin,
 1713 *Palaeogeography, Palaeoclimatology, Palaeoecology*, 181, 431–
 1714 452, doi:[https://doi.org/10.1016/S0031-0182\(01\)00444-8](https://doi.org/10.1016/S0031-0182(01)00444-8), URL
 1715 <https://www.sciencedirect.com/science/article/pii/S0031018201004448>,
 1716 2002
- 1717
- 1718 Pena, L. D. and Goldstein, S. L.: Thermohaline circulation crisis and impacts during the mid-
 1719 Pleistocene transition, *Science*, 345, 318–322, doi:10.1126/science.1249770, URL
 1720 <https://www.science.org/doi/abs/10.1126/science.1249770>, 2014.
- 1721



- 1722 Petersen, S. V., Schrag, D. P., and Clark, P. U.: A new mechanism for Dansgaard-Oeschger
 1723 cycles, *Paleoceanography*, 28, 24–30, doi:<https://doi.org/10.1029/2012PA002364>,
 1724 URL <https://agupubs.onlinelibrary.wiley.com/doi/abs/10.1029/2012PA002364>, 2013.
 1725
- 1726 Pol, K., Masson-Delmotte, V., Johnsen, S., Bigler, M., Cattani, O., Durand, G., Falourd, S.,
 1727 Jouzel, J., Minster, B., Parrenin, F., Ritz, C., Steen-Larsen, H., and Stenni, B.: New
 1728 MIS 19 EPICA Dome C high resolution deuterium data: Hints for a problematic
 1729 preservation of climate variability at sub-millennial scale in the “oldest ice”, *Earth*
 1730 *and Planetary Science Letters*, 298, doi:10.1016/J.EPSL.2010.07.030, 2010.
 1731
- 1732 Poppelmeier, F., Scheen, J., Jeltsch-Thommes, A., and Stocker, T. F.: Simulated stability of
 1733 the Atlantic Meridional Overturning Circulation during the Last Glacial Maximum,
 1734 *Climate of the Past*, 17, 615–632, doi:10.5194/cp-17-615-2021, URL
 1735 <https://cp.copernicus.org/articles/17/615/2021/>, 2021.
 1736
- 1737 Primeau, F. and Deleersnijder, E.: On the time to tracer equilibrium in the global
 1738 ocean, *Ocean Science*, 5, 13–28, doi:10.5194/os-5-13-2009, URL
 1739 <https://os.copernicus.org/articles/5/13/2009/>, 2009.
 1740
- 1741 Rahmstorf, S., Crucifix, M., Ganopolski, A., Goosse, H., Kamenkovich, I., Knutti, R.,
 1742 Lohmann, G., Marsh, R., Mysak, L., Wang, Z., and Weaver, A.: Thermohaline
 1743 circulation hysteresis: A model intercom- parison, *Geophysical Research Letters*, 322,
 1744 doi:10.1029/2005GL023655, 2005.
 1745
- 1746 Railsback, L., Gibbard, P., Head, M., Voarintsoa, N. R., and Toucanne, S.: An optimized
 1747 scheme of lettered marine isotope substages for the last 1.0 million years, and
 1748 the climatostratigraphic nature of isotope stages and substages, *Quaternary Science*
 1749 *Reviews*, 111, 94–106, doi:10.1016/j.quascirev.2015.01.012, 2015.
 1750
- 1751 Raymo, M., Ganley, K., Carter, S., Oppo, D., and McManus, J.: Millennial-scale instability
 1752 during the early Pleistocene epoch, *Nature*, 392, 699–702, doi:10.1038/33658, 1998.
 1753
- 1754 Raymo, M. E.: The timing of major climate terminations, *Paleoceanography*, 12, 577–585,
 1755 doi:<https://doi.org/10.1029/97PA01169>, URL
 1756 <https://agupubs.onlinelibrary.wiley.com/doi/abs/10.1029/97PA01169>, 1997.
 1757
- 1758 Raymo, M. E. and Nisancioglu, K. H.: The 41 kyr world: Milankovitch’s other unsolved
 1759 mystery, *Paleoceanography*, 18, doi:<https://doi.org/10.1029/2002PA000791>, URL
 1760 <https://agupubs.onlinelibrary.wiley.com/doi/abs/10.1029/2002PA000791>, 2003.
 1761
- 1762 Raymo, M. E., Oppo, D. W., and Curry, W.: The Mid-Pleistocene climate transition: A
 1763 deep sea carbon isotopic perspective, *Paleoceanography*, 12, 546–559,
 1764 doi:<https://doi.org/10.1029/97PA01019>, URL
 1765 <https://agupubs.onlinelibrary.wiley.com/doi/abs/10.1029/97PA01019>, 1997.
 1766
- 1767 Rhines, A. and Huybers, P.: Estimation of spectral power laws in time uncertain series of data
 1768 with application to the Greenland Ice Sheet Project $\delta^{18}\text{O}$ record, *Journal of*
 1769 *Geophysical Research: Atmospheres*, 116, doi:<https://doi.org/10.1029/2010JD014764>,
 1770 URL <https://agupubs.onlinelibrary.wiley.com/doi/abs/10.1029/2010JD014764>, 2011.
 1771



- Rodrigues, T., Alonso-García, M., Hodell, D., Rufino, M., Naughton, F., Grimalt, J., Voelker, A., and Abrantes, F.: A 1-Ma record of sea surface temperature and extreme cooling events in the North Atlantic: A perspective from the Iberian Margin, *Quaternary Science Reviews*, 172, 118–130, doi:https://doi.org/10.1016/j.quascirev.2017.07.004, URL https://www.sciencedirect.com/science/article/pii/S027737911630590X, 2017.
- Sakai, K. and Peltier, W. R.: A dynamical systems model of the Dansgaard–Oeschger oscillation and the origin of the Bond Cycle, *Journal of Climate*, 12, 2238–2255, doi:10.1175/1520-0442, URL https://journals.ametsoc.org/view/journals/clim/12/8/1520-044219990122238adsmot2
- Sanchez Goni, M., Rodrigues, T., Hodell, D., Polanco-Martínez, J., Alonso-García, M., Hernández-Almeida, I., Desprat, S., and Ferretti, P.: Tropically-driven climate shifts in southwestern Europe during MIS 19, a low eccentricity interglacial, *Earth and Planetary Science Letters*, 448, 81–93, doi:https://doi.org/10.1016/j.epsl.2016.05.018, URL https://www.sciencedirect.com/science/article/pii/S0012821X16302357, 2016.
- Sevellec, F. and Fedorov, A. V.: Unstable AMOC during glacial intervals and millennial variability: The role of mean sea ice extent, *Earth and Planetary Science Letters*, 429, 60–68, doi:https://doi.org/10.1016/j.epsl.2015.07.022, URL https://www.sciencedirect.com/science/article/pii/S0012821X15004495, 2015.
- Shackleton, N., Fairbanks, R., Chien Chiu, T., and Parrenin, F.: Absolute calibration of the Greenland time scale: implications for Antarctic time scales and for ^{14}C , *Quaternary Science Reviews*, 23, 1513–1522, doi:https://doi.org/10.1016/j.quascirev.2004.03.006, URL https://www.sciencedirect.com/science/article/pii/S0277379104000824, 2004.
- Shackleton, N. J., Hall, M. A., and Vincent, E.: Phase relationships between millennial-scale events 64,000–24,000 years ago, *Paleoceanography*, 15, 565–569, doi:https://doi.org/10.1029/2000PA000513, URL https://agupubs.onlinelibrary.wiley.com/doi/abs/10.1029/2000PA000513, 2000.
- Shin, J., Nehrbass-Ahles, C., Grilli, R., Chowdhry Beeman, J., Parrenin, F., Teste, G., Landais, A., Schmidely, L., Silva, L., Schmitt, J., Bereiter, B., Stocker, T. F., Fischer, H., and Chappellaz, J.: Millennial-scale atmospheric CO_2 variations during the Marine Isotope Stage 6 period (190–135 ka), *Climate of the Past*, 16, 2203–2219, doi:10.5194/cp-16-2203-2020, URL https://cp.copernicus.org/articles/16/2203/2020/, 2020.
- Siddall, M., Rohling, E. J., Thompson, W. G., and Waelbroeck, C.: Marine isotope stage 3 sea level fluctuations: Data synthesis and new outlook, *Reviews of Geophysics*, 46, doi:https://doi.org/10.1029/2007RG000226, URL https://agupubs.onlinelibrary.wiley.com/doi/abs/10.1029/2007RG000226, 2008.
- Sima, A., Paul, A., and Schulz, M.: The Younger Dryas - An intrinsic feature of late Pleistocene climate change at millennial timescales, *Earth and Planetary Science Letters*, 222, 741–750, doi:10.1016/j.epsl.2004.03.026, 2004.



- 1822
 1823 Skinner, L. and McCave, I.: Analysis and modeling of gravity and piston coring based on soil
 1824 mechanics, *Marine Geology*, 199, 181–204, doi:10.1016/S0025-3227(03)00127-0,
 1825 2003.
 1826
 1827 Skinner, L. and Shackleton, N.: An Atlantic lead over Pacific deep-water change across
 1828 Termination I: implications for the application of the marine isotope stage
 1829 stratigraphy, *Quaternary Science Reviews*, 24, 571–
 1830 580, doi:https://doi.org/10.1016/j.quascirev.2004.11.008, URL
 1831 https://www.sciencedirect.com/science/article/pii/S0277379104003336,
 1832 2005.
 1833
 1834 Skinner, L. and Shackleton, N.: Deconstructing Terminations I and II: Revisiting the
 1835 glacioeustatic paradigm based on deep-water temperature estimates, *Quaternary*
 1836 *Science Reviews*, 25, 3312–3321, doi:10.1016/j.quascirev.2006.07.005, 2006.
 1837
 1838 Skinner, L. C., Shackleton, N. J., and Elderfield, H.: Millennial-scale variability of deep-
 1839 water temperature and $^{18}\text{O}_{\text{dw}}$ indicating deep-water source variations in the Northeast
 1840 Atlantic, 0–34 cal. ka BP, *Geochemistry, Geophysics, Geosystems*, 4,
 1841 doi:https://doi.org/10.1029/2003GC000585, URL
 1842 https://agupubs.onlinelibrary.wiley.com/doi/abs/10.1029/2003GC000585, 2003.
 1843
 1844 Skinner, L. C., Elderfield, H., and Hall, M.: Phasing of millennial climate events and
 1845 northeast Atlantic Deep-Water temperature change since 50 Ka BP, pp. 197–208,
 1846 American Geophysical Union (AGU), doi:https://doi.org/10.1029/173GM14, URL
 1847 https://agupubs.onlinelibrary.wiley.com/doi/abs/10.1029/173GM14, 2007.
 1848
 1849 Skinner, L. C., Fallon, S., Waelbroeck, C., Michel, E., and Barker, S.: Ventilation of the deep
 1850 Southern Ocean and deglacial CO_2 rise, *Science*, 328, 1147–
 1851 1151, doi:10.1126/science.1183627, URL
 1852 https://www.science.org/doi/abs/10.1126/science.1183627, 2010.
 1853
 1854 Skinner, L., Menviel, L., Broadfield, L., Gottschalk, J., and Greaves,
 1855 M.: Southern Ocean convection amplified past Antarctic warming
 1856 and atmospheric CO_2 rise during Heinrich Stadial 4, *Communications*
 1857 *Earth & Environment*, 1, 23, doi:10.1038/s43247-020-00024-3, URL
 1858 https://doi.org/10.1038/s43247-020-00024-3, 2020.
 1859
 1860 Stocker, T. F.: The Seesaw Effect, *Science*, 282, 61–62, doi:10.1126/science.282.5386.61,
 1861 URL https://www.science.org/doi/abs/10.1126/science.282.5386.61, 1998.
 1862
 1863 Stocker, T. F. and Johnsen, S. J.: A minimum thermodynamic model for the bipolar seesaw,
 1864 *Paleoceanography*, 18, doi:https://doi.org/10.1029/2003PA000920, URL
 1865 https://agupubs.onlinelibrary.wiley.com/doi/abs/10.1029/2003PA000920, 2003.
 1866
 1867 Sun, Y., McManus, J. F., Clemens, S. C., Zhang, X., Vogel, H., Hodell, D. A., Guo, F.,
 1868 Wang, T., Liu, X., and An, Z.: Persistent orbital influence on millennial climate
 1869 variability through the Pleistocene, *Nature Geoscience*, 14, 812–818,
 1870 doi:10.1038/s41561-021-00794-1, URL https://doi.org/10.1038/s41561-021-00794-1,
 1871 2021.



- 1872
 1873 Thomas, N.C., Bradbury, H.J., and Hodell, D.A.: Changes in North Atlantic deep-water
 1874 oxygenation across the Middle Pleistocene Transition, *Science*,
 1875 [science.org/doi/10.1126/science.abj7761](https://doi.org/10.1126/science.abj7761), 2022.
 1876
 1877 Timmermann, A., Gildor, H., Schulz, M., and Tziperman, E.: Coherent resonant millennial-
 1878 scale climate oscillations triggered by massive meltwater pulses, *Journal of Climate*,
 1879 16, 2569 – 2585, doi:10.1175/1520-0442, URL
 1880 <https://journals.ametsoc.org/view/journals/clim/16/15/1520-044220030162569crmcot>,
 1881 2003.
 1882
 1883 Tüenter, E., Weber, S. L., Hilgen, F. J., and Lourens, L. J.: Sea-ice feedbacks on
 1884 the climatic response to precession and obliquity forcing, *Geophysical*
 1885 *Research Letters*, 32, doi:<https://doi.org/10.1029/2005GL024122>, URL
 1886 <https://agupubs.onlinelibrary.wiley.com/doi/abs/10.1029/2005GL024122>,
 1887 2005.
 1888
 1889 Tzedakis, P., Margari, V., and Hodell, D.: Coupled ocean–land millennial-scale changes
 1890 1.26 million years ago, recorded at Site U1385 off Portugal, *Global and Planetary*
 1891 *Change*, 135, 83– 88, doi:<https://doi.org/10.1016/j.gloplacha.2015.10.008>, URL
 1892 <https://www.sciencedirect.com/science/article/pii/S0921818115300850>, 2015.
 1893
 1894 Tzedakis, P. C., Drysdale, R. N., Margari, V., Skinner, L. C., Menviel, L., Rhodes, R. H.,
 1895 Taschetto, A. S., Hodell, D. A., Crowhurst, S. J., Hellstrom, J. C., Fallick, A.
 1896 E., Grimalt, J. O., McManus, J. F., Martrat, B., Mokeddem, Z., Parrenin, F.,
 1897 Regattieri, E., Roe, K., and Zanchetta, G.: Enhanced climate instability in the North
 1898 Atlantic and southern Europe during the Last Interglacial, *Nature Communications*, 9,
 1899 4235, doi:10.1038/s41467-018-06683-3, URL [https://doi.org/10.1038/s41467-018-](https://doi.org/10.1038/s41467-018-06683-3)
 1900 [06683-3](https://doi.org/10.1038/s41467-018-06683-3), 2018.
 1901
 1902 Vautravers, M. J. and Shackleton, N. J.: Centennial-scale surface hydrology off Portugal
 1903 during marine isotope stage 3: Insights from planktonic foraminiferal fauna
 1904 variability, *Paleoceanography*, 21, doi:<https://doi.org/10.1029/2005PA001144>, URL
 1905 <https://agupubs.onlinelibrary.wiley.com/doi/abs/10.1029/2005PA001144>, 2006.
 1906
 1907 Verbitsky, M. Y., Crucifix, M., and Volobuev, D. M.: A theory of Pleistocene glacial
 1908 rhythmicity, *Earth System Dynamics*, 9, 1025–1043, doi:10.5194/esd-9-1025-2018,
 1909 URL <https://esd.copernicus.org/articles/9/1025/2018/>, 2018.
 1910
 1911 Vettoretti, G., Ditlevsen, P., Jochum, M., and Rasmussen, S. O.: Atmospheric CO₂ control of
 1912 spontaneous millennial-scale ice age climate oscillations, *Nature Geoscience*, 15,
 1913 300–306, doi:10.1038/s41561-022-00920-7, URL [https://doi.org/10.1038/s41561-](https://doi.org/10.1038/s41561-022-00920-7)
 1914 [022-00920-7](https://doi.org/10.1038/s41561-022-00920-7), 2022.
 1915
 1916 Vimeux, F., Masson, V., Jouzel, J., Stievenard, M., and Petit, J. R.: Glacial–interglacial
 1917 changes in ocean surface conditions in the Southern Hemisphere, *Nature*, 398, 410–
 1918 413, doi:10.1038/18860, URL <https://doi.org/10.1038/18860>, 1999.
 1919
 1920 Waelbroeck, C., Skinner, L. C., Labeyrie, L., Duplessy, J.-C., Michel, E., Vazquez Riveiros,
 1921 N., Gherardi, J.-M., and Dewilde, F.: The timing of deglacial circulation changes in



- 1922 the Atlantic, *Paleoceanography*, 26, doi:<https://doi.org/10.1029/2010PA002007>, URL
 1923 <https://agupubs.onlinelibrary.wiley.com/doi/abs/10.1029/2010PA002007>,
 1924 2011
- 1925
 1926
- 1927 WAIS Divide Project Members: Precise inter polar phasing of abrupt climate change during
 1928 the last ice age, *Nature*, 520, 661–665, doi:10.1038/nature14401, URL
 1929 <https://doi.org/10.1038/nature14401>, 2015.
- 1930
- 1931 Weirauch, D., Billups, K., and Martin, P.: Evolution of millennial-scale climate variability
 1932 during the mid-Pleistocene, *Paleoceanography*, 23,
 1933 doi:<https://doi.org/10.1029/2007PA001584>, URL
 1934 <https://agupubs.onlinelibrary.wiley.com/doi/abs/10.1029/2007PA001584>, 2008.
- 1935
- 1936 Winton, M. and Sarachik, E. S.: Thermohaline oscillations induced by strong steady salinity
 1937 forcing of ocean general circulation models, *Journal of Physical Oceanography*, 23,
 1938 1389–1410, doi:10.1175/1520-0485, URL
 1939 [https://journals.ametsoc.org/view/journals/phoc/23/7/1520-](https://journals.ametsoc.org/view/journals/phoc/23/7/1520-048519930231389toibss20c)
 1940 [048519930231389toibss20c](https://journals.ametsoc.org/view/journals/phoc/23/7/1520-048519930231389toibss20c)
- 1941
- 1942 Wolff, E. W., Fischer, H., and Rothlisberger, R.: Glacial terminations as southern
 1943 warmings without northern control, *Nature Geoscience*, 2, 206–209, doi:
 1944 10.1038/ngeo442, URL <https://doi.org/10.1038/ngeo442>, 2009.
- 1945
- 1946 Wolff, E. W., Fischer, H., van Ommen, T., and Hodell, D. A.: Stratigraphic templates for
 1947 ice core records of the past 1.5 million years, *Climate of the Past Discussions*,
 1948 2022, 1–22, doi:10.5194/cp-2022-2, URL [https://cp.copernicus.org/preprints/cp-2022-](https://cp.copernicus.org/preprints/cp-2022-2/)
 1949 [2/](https://cp.copernicus.org/preprints/cp-2022-2/), 2022.
- 1950
- 1951 Yan, Y., Bender, M. L., Brook, E. J., Clifford, H. M., Kemeny, P. C., Kurbatov, A. V.,
 1952 Mackay, S., Mayewski, P. A., Ng, J., Severinghaus, J. P., and Higgins, J. A.: Two-
 1953 million-year-old snapshots of atmospheric gases from Antarctic ice, *Nature*, 574,
 1954 663–666, doi:10.1038/s41586-019-1692-3, URL [https://doi.org/10.1038/s41586-019-](https://doi.org/10.1038/s41586-019-1692-3)
 1955 [1692-3](https://doi.org/10.1038/s41586-019-1692-3), 2019.
- 1956
- 1957 Yin, Q. Z., Wu, Z. P., Berger, A., Goosse, H., and Hodell, D.: Insolation triggered abrupt
 1958 weakening of Atlantic circulation at the end of interglacials, *Science*, 373, 1035–
 1959 1040, doi:10.1126/science.abg1737, URL
 1960 <https://www.science.org/doi/abs/10.1126/science.abg1737>, 2021.
- 1961
- 1962 Zhang, X., Lohmann, G., Knorr, G., and Purcell, C.: Abrupt glacial climate shifts
 1963 controlled by ice sheet changes, *Nature*, 512, 290–294, doi: 10.1038/nature13592,
 1964 URL <https://doi.org/10.1038/nature13592>, 2014.
- 1965
- 1966 Zhang, X., Knorr, G., Lohmann, G., and Barker, S.: Abrupt North Atlantic circulation
 1967 changes in response to gradual CO₂ forcing in a glacial climate state, *Nature*
 1968 *Geoscience*, 10, 518–523, doi:10.1038/ngeo2974, URL
 1969 <https://doi.org/10.1038/ngeo2974>, 2017.
- 1970



- 1971 Zhang, X., Barker, S., Knorr, G., Lohmann, G., Drysdale, R., Sun, Y., Hodell, D., and Chen,
 1972 F.: Direct astronomical influence on abrupt climate variability, *Nature Geoscience*,
 1973 14, 819–826, doi:10.1038/s41561-021-00846-6, URL
 1974 <https://doi.org/10.1038/s41561-021-00846-6>, 2021.
 1975
 1976 Zitellini, N., Gracia, E., Matias, L., Terrinha, P., Abreu, M., DeAlteriis, G., Henriët, J.,
 1977 Danobeitia, J., Masson, D., Mulder, T., Ramella, R., Somoza, L., and Diez, S.: The
 1978 quest for the Africa–Eurasia plate boundary west of the Strait of Gibraltar, *Earth and*
 1979 *Planetary Science Letters*, 280, 13–50, doi:<https://doi.org/10.1016/j.epsl.2008.12.005>,
 1980 URL <https://www.sciencedirect.com/science/article/pii/S0012821X0800753X>, 2009.
 1981